IDŐJÁRÁS

QUARTERLY JOURNAL
OF THE HUNGARIAN METEOROLOGICAL SERVICE

CONTENTS

****

http://omsz.met.hu/omsz.php?almenu_id=omsz&pid=references&pri=2

VOL. 110 * NO. 1 * JANUARY - MARCH 2006

IDŐJÁRÁS

Quarterly Journal of the Hungarian Meteorological Service

Editorial Office: P.O. Box 39, H-1675 Budapest, Hungary or
Gilice tér 39, H-1181 Budapest, Hungary
E-mail: bozo.l@met.hu or *antal.e@met.hu*
Fax: (36-1) 346-4809

Subscription by

mail: IDŐJÁRÁS, P.O. Box 39, H-1675 Budapest, Hungary;
E-mail: bozo.l@met.hu or *antal.e@met.hu*; *Fax: (36-1) 346-4809*

IDŐJÁRÁS

Quarterly Journal of the Hungarian Meteorological Service
Vol. 110, No. 1, January–March 2006, pp. 1–13

Characteristics and synoptic classification of heavy snowfall events in Budapest for the period 1953–2003 Part I

György Babolcsai and **Tamás Hirsch**

Hungarian Meteorological Service
P.O. Box 38, H-1525 Budapest, Hungary; E-mail: babolcsai.gy@met.hu

(Manuscript received in final form January 16, 2006)

Abstract—Winter precipitation is one of the most challenging meteorological phenomena for operational weather forecasters. A possible way of increasing forecast skill is to investigate cases occurred in the past, trying to find essential processes as well as important parameters, and to draw conclusions based on the results. Heavy snowfall events have been investigated for the period 1953–2003 in Budapest. After providing a precise definition of heavy snowfall events, SYNOP reports for the station Pestlőrinc (Budapest) as well as data from the NCEP/NCAR Reanalysis dataset with a temporal resolution of 6 hours have been collected for each event. Based on this comprehensive database, two types of investigation have been carried out. The first part of the paper contains the main characteristics of heavy snowfall events, while in Part II, results connected with the subjective classification of the cases will be presented. The length of the investigated period (50 years) makes it possible to seek potential signs of climate change as well. One of the most important results of the first part of the study is the high stability of the climate system in terms of heavy snowfall events in Budapest. In most of the characteristics, there has been only a slight change during the past 50 years. The most important change revealed by the research, however, is the considerable modification of the frequency of heavy snowfall events within the winter period itself. It can be also stated that our results could be efficiently used in operational weather forecasting.

Key-words: synoptic climatology, heavy snowfall events, snowfall characteristics

1. Introduction

Heavy snowfall events and blizzards are one of those situations still capable of causing huge problems. There are much more devastating weather phenomena as well (e.g., hurricanes, tornadoes, some convective events in summer), but

heavy snowfall events are either much more frequent or cover larger areas, or last longer. In Hungary, these events play a basic role in this respect besides flooding. Therefore, even nowadays it is of vital importance to investigate the conditions leading to heavy snowfall as well as to determine their characteristics, thereby improving their forecasts.

One fifth of Hungary's population lives in a relatively small area, in its capital, Budapest. This well-known fact makes forecasts prepared for this region very important. Even if the weather forecast valid for the country is of basically good quality, it is regarded as unsuccessful by major part of the population if something unexpected occurs in the capital city alone. An unpredicted snowfall in Budapest is one of those situations that will lead to negative response from the public. The reason for this is mainly that in the winter season, people are mostly interested in the question whether it will be snowing and how much.

The synoptic station in Pestlőrinc (Budapest) has been providing data since 1953, so it was possible to investigate heavy snowfall cases based on a 50-year period. The selected station, situated at a height of 140 m above mean sea level, is representative of the snow conditions of the major part of the city.

Heavy snowfall events have been defined as cases of continuous snowfall resulting in a snow cover depth increase exceeding 8 cm. Because of the lower spatial variability of precipitation amount during winter, the formation of a considerable snow cover is also likely in other parts of the city in the selected cases. Important characteristics of heavy snowfall events (HSEs) have been determined and HSEs have been classified as well according to several aspects. This is useful, because the frequency of such events can be estimated in case of given synoptic situations and whether there is any difference in the characteristics of heavy snowfall events depending on their type. In this first part of the paper, the most important characteristics of HSEs will be presented, while the second part is devoted to showing the results connected to the classification of cases.

2. Background

Investigation methods of HSEs show a great variability. Even the definition of cases to be investigated can be quite different. *Spreitzhofer* (1999a) selected cases, when the 24-hour increase in snow cover depth was at least 20 cm in at least 3 of the 81 Austrian stations below 1500 m (above mean sea level). *Younkin*'s studies (*Goree* and *Younkin*, 1966; *Younkin*, 1968) included cases with a snow cover increase of at least 10 cm in an area covering geographical latitudes of at least 6° in the USA. *Wild et al.* (1996) studied blizzards

(moderate or heavy snowfall accompanied by winds of at least 30 knots (~15 m/s) causing snow drift and decreasing visibility below 200 m) using the UK Met Office's definition from 1991. *McNulty* (1991) investigated snowfall events producing a snow cover of at least 5 cm in 12 hours in the area of the Great Lakes in the US, and found 5 synoptic situations with heavy snowfall. *Böhm* (1975) studied cases with at least 5 cm snow cover increase in 24 hours in Vienna.

Besides the selection of cases, the investigation itself can be quite different as well. *Younkin* (*Goree* and *Younkin*, 1966; *Younkin*, 1968) separated 3 weather types based on the circulation conditions at 500 hPa level, focusing mainly on the location and value of the absolute vorticity maxima.

According to *Schalko* (1949), HSEs in the Northern Alps are caused by the orography in case of strong and moist northwesterly flow. The Southern Alps similarly to Eastern Austria can get large amounts of snow in the warm sector of cyclones with centre over Genova. Much more infrequently, cold surges from the east can also result in snowstorms over Austria.

Spreitzhofer (1999a) carried out investigations into the spatial, temporal, and intensity characteristics of HSEs for the winters of 1970/71–1988/89 using daily snow data of 81 stations of the Austrian Hydrological Service. The author divided Austria into four parts, according to the main geographical directions. Spatial extent, eccentricity, and distance of the two furthest stations involved have been determined for each case. He found that in most cases, the zonal axis of the area with heavy snowfall is at least three times longer than its meridional axis, while the meridional axis is longer in only 6% of the cases. In an other study, *Spreitzhofer* (1999b) classified strong Austrian snowstorms from synoptic aspects based on 16 cases observed between 1986 and 1991, using satellite images and ECMWF model results as well.

Heavy snowfall intensity in the British Isles was studied by *Gray et al.* (1981) as the function of the effects resulting in the uprising motion of the air, which is the most important factor in the formation of precipitation. They found that in cyclonic situations, horizontal convergence results in an intensity of approximately 2.5 cm snow/hour, and the snowfall usually lasts for 6–12 hours. The presence of convective instability can produce an intensity of 4 cm/hour, limited to a short period of time and a small area. Frontal lifting leads to short but intense snowfall in case of cold fronts, whereas in case of warm fronts, more persistent but less intense snowfall can be observed due to the longer extent and slower motion of the frontal zone.

Wild et al. (1996) carried out investigations on blizzards developed in the area of the British Isles in the period of 1880–1989. Their results confirmed the essential role of front activity in the formation of heavy snowfall. 49% of the cases were due to warm front, 25% of the cases were caused by an occlusion,

18% by cold front, and only 8% were not connected to frontal activity. Cyclone trajectories were investigated for the period between 5 days prior and 5 days after the event, and a huge variability was found. The decade with the most blizzards was 1960–1969, and January turned out to be the month with the most frequent occurrence of cases.

Mote et al. (1997) studied synoptic characteristics of strong blizzards between 1960 and 1993 in the Southeastern US. Composite charts containing many meteorological parameters were constructed every 12 hours for the period of 72 hours prior to the onset of the event up to +48 hours. As a general conclusion, they stated that besides moist air from the Mexican Golf, blizzards mainly depend on warm air advection, upper level jets, diabatic processes, and cyclogenetic lifting.

Our investigation aims to fill the gap that exists in this important research area for Budapest for the previous 50 years.

3. Characteristics of heavy snowfall events in Budapest

Research has been carried out based on SYNOP reports of the station Pestlőrinc (Budapest), one of the main SYNOP stations of the Hungarian Meteorological Service. 50 winter periods (November, December, January, February, and March) have been investigated between 1953/54 and 2002/03. Heavy snowfall events (HSEs) have been defined as cases of continuous snowfall, producing a snow cover increase exceeding 8 cm at the mentioned station. These events should have produced considerable amount of snowfall in the whole area of Budapest. In case of similar investigations, it is usual to apply temporal or intensity limits. Our intention, however, was to study the weather systems themselves, so time (intensity) limits could not be applied due to the fact that snow depth measurements are only available two times a day (06 and 18 UTC).

Using SYNOP reports of the station Pestlőrinc (Budapest), the following characteristics have been assigned to each HSE:

- month of occurrence, duration, average intensity;
- snow depth increase, ratio of snow depth increase, and its water equivalent;
- average 2m temperature and mean sea level pressure during snowfall.

The other part of the database has been created using the NCEP/NCAR Reanalysis dataset available online at http://www.cdc.noaa.gov/cdc/data.-ncep.reanalysis.html. The NCEP/NCAR Reanalysis project is using a state-of-the-art analysis/forecast system to perform data assimilation from 1948 to the

present in order to create global fields of meteorological parameters with a temporal resolution of 6 hours. Reanalysis fields include surface, pressure level and tropopause level data, as well as various kinds of flux data. Using this dataset, average fields can be created for many meteorological parameters, arbitrary time periods, and any part of the world. Based on average fields created for each HSE (selected meteorological fields have been averaged for the duration of each event), the following characteristics have been determined for Budapest:

- average height of 500 hPa level;
- average total precipitable water;
- average temperature of 925 and 850 hPa levels.

Regarding winter periods from 1953/54 to 2002/03, 71 snowfall events resulting in a snow depth increase exceeding 8 cm have been found. The *number of cases* during the first 25 winter periods was 35, whereas during the next 25 years, 36 heavy snowfall events occurred, which means that there was only a slight difference. Monthly frequencies of HSEs are shown in *Table 1*.

Table 1. Number of heavy snowfall events

Period	November	December	January	February	March	Σ
1953/54–1977/78	4	8	12	8	3	35
1978/79–2002/03	9	10	6	8	3	36
1953/54–2002/03	13	18	18	16	6	71

For the investigated 50 years, December and January have turned out to be the months with the most cases (18 HSEs in each month) followed by February (16), November (13), and March (6). Comparing the two 25-year periods, it can be clearly seen that there was a significant increase in the number of cases in November, while in January significantly less HSE occurred in the second half of the investigated period. A slight increase in the frequency of HSEs has been experienced for December, and interestingly there was no change in case of February and March. Due to the mentioned changes, January, the month with the largest number of HSEs in the first 25 years, has become the month with the less cases excluding March.

According to *Fig. 1a,* the frequency distribution of *snow depth increase* caused by HSEs shows an approximately exponential decrease. During the

investigated 50 years, the largest increase of snow depth due to a HSE was 38 cm (November 29–December 1, 1980 and February 9–11, 1999). Median of all events is 13 cm, while the average is 15 cm. As shown in *Table 2*, there is an increase in the average value by more than 2 cm from the first to the second half of the investigated period. The month with the largest increase in snow depth on average is January. Interestingly, the average increase for November is greater than for December, possibly due to the larger precipitation amounts in the former month. Looking at the mean absolute deviation values, it can be stated that February was the month with the largest and March with the smallest variability during the 50 years.

Another important characteristic of HSEs is their *duration*. The shortest event lasted only for 3 hours resulting in a snow depth increase of 10 cm, while the longest HSE brought 26 cm of snow in 53 hours. The hours at the beginning and end of the heavy snowfall event with precipitation amount less than 0.1 mm have not been included. The median of the duration of heavy snowfall events is 17 hours, and the average is 20 hours. According to *Fig. 1b*, the category 12–18 hours was the most frequent, and the distribution is definitely positively skewed. The average duration of HSEs has slightly increased during the investigated period (*Table 2*). The high average value for March might seem interesting at first sight. This is obviously due to the fact, that stronger solar radiation and higher temperatures which are characteristic of this month enable the snow cover increase to exceed 8 cm, mostly only in case of longer snowfall events with overcast sky, when during the day the solar radiation strongly decreased prohibiting the melting of snow. January has turned out to be the month with the lowest and February with the highest variability of snowfall duration.

Snowfall intensity is also worth studying (*Fig. 1c*). The lowest average intensity during the 50 years was 0.2 cm/hour caused by a snowfall event lasting for 2 days, resulting in a snow depth increase of 10 cm. The case with the highest intensity, namely 3.3 cm/hour, also brought 10 cm of snow but within only 3 hours. The median of average snowfall intensity has been determined as 0.8 cm/hour, while the average value has turned out to be 0.9 cm/hour. According to *Fig. 1c*, average snowfall intensity has a bimodal distribution with both the category of 0.4–0.6 cm/hour and 0.8–1.0 cm/hour, having approximately the same relative frequency of about 25%. There is hardly any change in the average intensity values of the two halves of the investigated period (*Table 2*). Snowfall intensity is near 1 cm/hour on average in every month except for March, which is characterized by an average of about 0.5 cm/hour, most probably due to the considerably higher degree of melting during snowfall events in this month compared to the others.

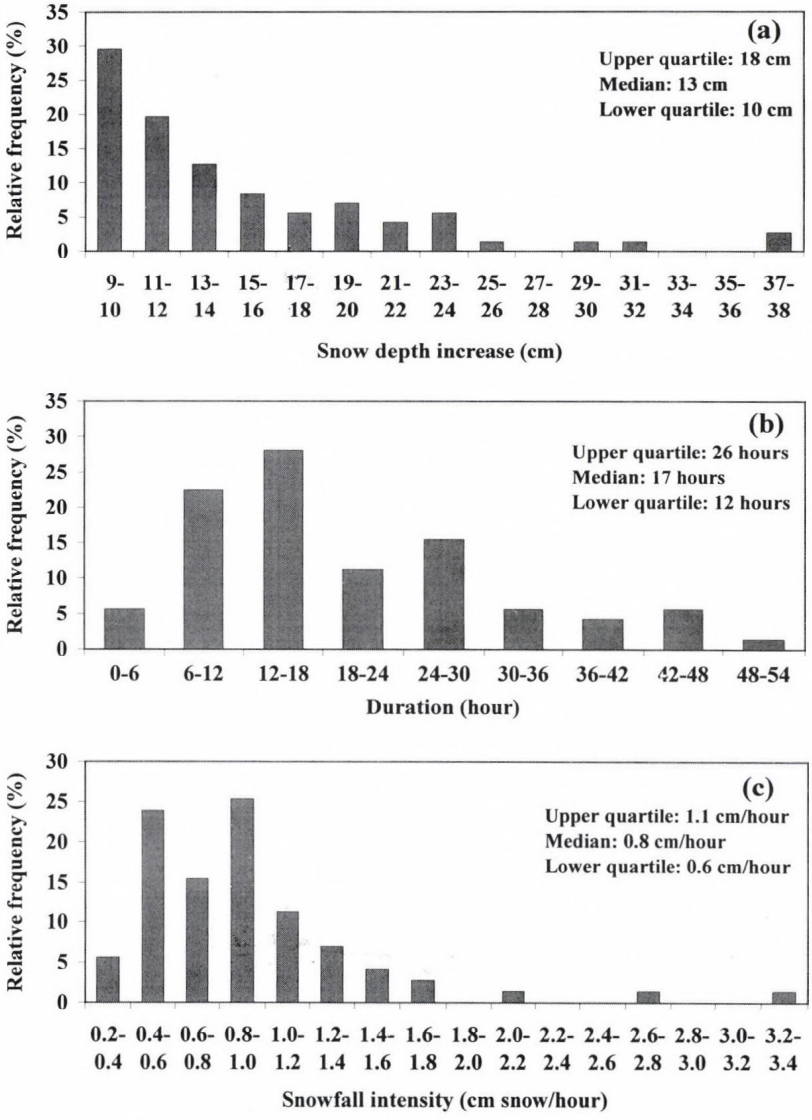

Fig. 1. Frequency distribution of snow depth increase (a), duration (b), and average snowfall intensity (c) for heavy snowfall events.

In *Fig. 2a*, *the ratio of snow depth increase and its water equivalent* is shown, which falls into the category of 0.9–1.2 cm/mm in nearly 50% of the cases. The distribution is positively skewed with a median of 1.1 cm/mm and an average of 1.3 cm/mm. According to *Table 2*, both average and mean

absolute deviation have decreased during the investigated period. Monthly averages show, that a precipitation amount of 1 mm approximately corresponds to 1 cm of snow in November, December, and March, while the same amount of precipitation is equivalent to nearly 1.5 cm of snow in January and February.

Table 2. Characteristics of heavy snowfall events: average (upper corner) and mean absolute deviation (lower corner)

	1953/54–2002/03	**1953/54–1977/78**	**1978/79–2002/03**	**Nov**	**Dec**	**Jan**	**Feb**	**Mar**
Snow depth increase (cm)	15.0 5.0	13.8 4.3	16.1 5.6	15.1 4.6	13.9 3.9	16.8 4.6	15.8 6.9	10.0 0.7
Duration (h)	20 9	19 8	21 10	18 8	19 9	22 7	19 11	25 9
Snowfall intensity (cm/h)	0.92 0.36	0.94 0.41	0.9 0.31	1.05 0.46	0.87 0.32	0.96 0.36	0.98 0.32	0.48 0.17
Ratio of snow depth incr. and its water equiv. (cm/mm)	1.26 0.33	1.31 0.37	1.2 0.29	1.15 0.26	1.1 0.26	1.46 0.34	1.41 0.36	0.9 0.21
Total precipitable water (mm)	11.6 1.7	11.8 1.7	11.4 1.6	12.3 2.0	11.6 1.7	10.9 1.1	11.3 1.8	13.3 1.1
Mean sea level pressure (hPa)	1009 7.2	1008 6.8	1009 7.7	1014 7.4	1007 7.0	1008 8.3	1006 5.8	1010 5.7
Height of 500 hPa level (gpm)	5380 67	5379 63	5382 72	5425 94	5369 46	5364 71	5358 62	5427 34
2m temperature (°C)	–2.5 2.0	–2.5 1.8	–2.6 2.2	–1.4 1.1	–2.5 1.9	–3.6 2.2	–2.9 2.4	–0.9 1.0
Temperature at the 925 hPa level (°C)	–3.5 2.6	–3.2 2.2	–3.8 3.0	–2.6 1.8	–3.6 2.7	–4.6 3.4	–3.9 2.5	–1.2 1.8
Temperature at the 850 hPa level (°C)	–4.9 2.3	–4.9 2.2	–5.0 2.5	–4.2 1.6	–4.9 2.5	–5.9 2.6	–5.1 2.1	–3.2 1.5

Heavy snowfall events are caused by cyclones, so it is worth having a look at the *mean sea level pressure* (MSLP) as well. The lowest average MSLP during HSEs was 987 hPa, in case of a deep secondary low on December 28, 1999. The highest average MSLP, namely 1028 hPa, was connected to a case on January 19, 1995, when a shallow cyclone developed over Italy between a huge cyclone over the Atlantic and an anticyclone in Eastern Europe. Most frequently, the category of 1005–1010 hPa occurred (*Fig. 2b*) where median (1008 hPa) and average (1009 hPa) can also be found, pointing to the rather high degree of symmetry of the distribution. There is hardly any difference in the average value characteristic of the two halves of the investigated period (*Table 2*). November has turned out to be the month

with the highest average MSLP during heavy snowfall events, while January is the month with the largest variability.

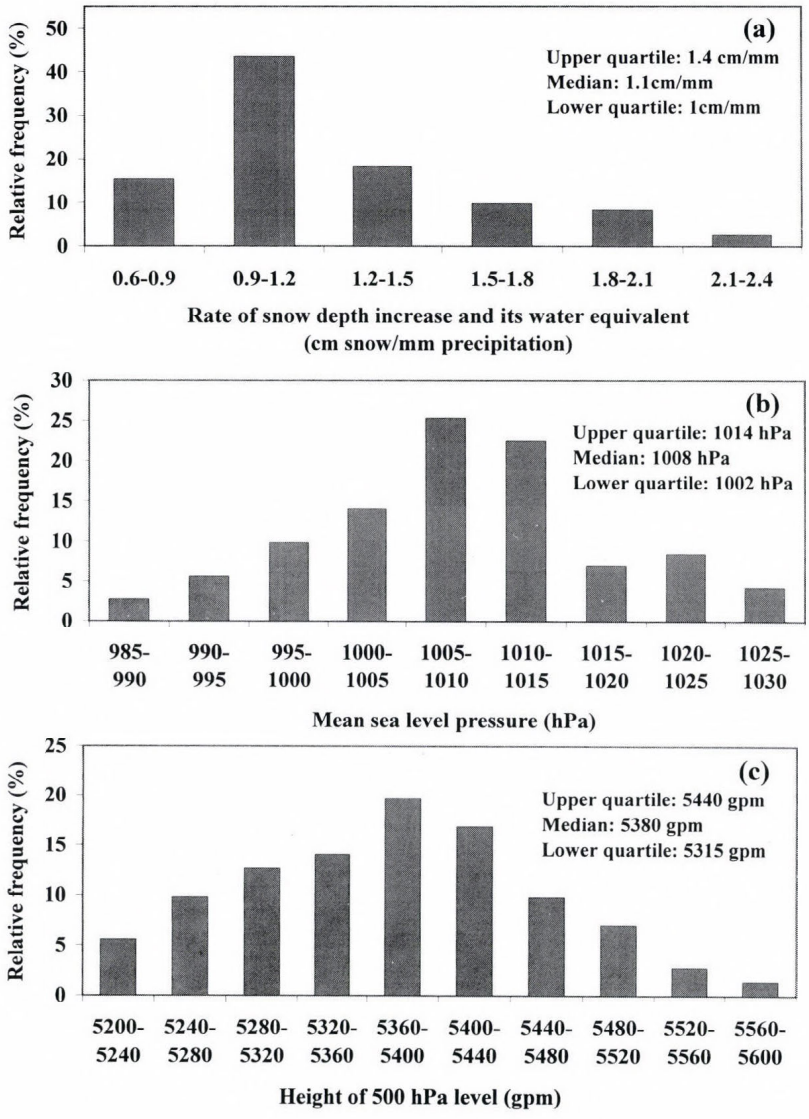

Fig. 2. Frequency distribution of the rate of snow depth increase and its water equivalent (a), mean sea level pressure (b), and the average height of 500 hPa level (c) for heavy snowfall events.

While MSLP characterizes weather systems near the surface, the *height of 500 hPa level* is used to get upper level information. The lowest average value during HSEs for this parameter was 5220 gpm, the highest value reached 5590 gpm. As shown in *Fig. 2c*, the frequency of average height continuously increases up to the category of 5360–5400 gpm, followed by a steady decrease towards higher values. Both average and median are 5380 gpm. Looking at monthly means (*Table 2*), it can be seen that there is a gradual decrease from November till February followed by a sudden increase in March, when the average value is very close to that calculated for November. Variability is the highest in November, and there is only very little change in the average during the investigated 50 years.

One of the key parameters when investigating heavy snowfall events is *total precipitable water* (PW), showing the amount of precipitation that would result from the condensation of all the water vapor contained by the air column above a given point. Obviously, higher PW values favor the development of heavy precipitation. On the other hand, precipitation in form of snow requires low temperatures, which strongly limits possible maximum values of precipitable water, even if the whole layer above surface is close to being saturated. PW values averaged for the duration of HSEs are shown in *Fig. 3a*. The distribution is very symmetric with both the median and average being 12 mm. The lowest mean precipitable water, namely only 6 mm, was connected to the formation of a strong convergence zone along the Danube on 13 December, 2001, resulting in 13 cm of snow for the next morning. The highest average PW value during heavy snowfall was 17 mm, associated with a case on November 18–20, 1965, when very moist air from the south streamed over the Carpathian Basin in the warm sector of a cyclone with centre over the British Isles. According to *Table 2*, the average PW gradually decreases until January, followed by an increase in the consecutive months.

2m temperature averaged for the period of HSEs has also been investigated (*Fig. 3b*). 50% of the cases fell between 0 and –2 °C, and average temperature above 0 °C occurred only 4 times during the investigated 50 years. The lowest average of 2m temperature was –10 °C. The frequency distribution is negatively skewed with a median of –1.8 °C and an average of –2.5 °C. In the distribution, there is a secondary maximum at –6 °C. According to *Table 2*, the average values for the two 25-year periods are almost the same, and there is a slight increase in the mean absolute deviation in the second half of the investigated period. According to *Böhm*'s research (1975), the mean temperature in Vienna during heavy snowfall is mostly between 0 and –0.9 °C.

As last characteristic, *average temperature of the 850 and 925 hPa levels* are shown in *Fig. 3c*. In 25% of the cases, the average of the 850 hPa level temperature is –3 °C, which is the most frequent value for 925 hPa as well.

In case of 850 hPa level temperature, positive average value did not occur during the 50 years, the median was –4 °C, whereas the average was –5 °C. Its frequency distribution shows a definite bimodality with a second maximum at –6 °C, at the same value as 2m temperature.

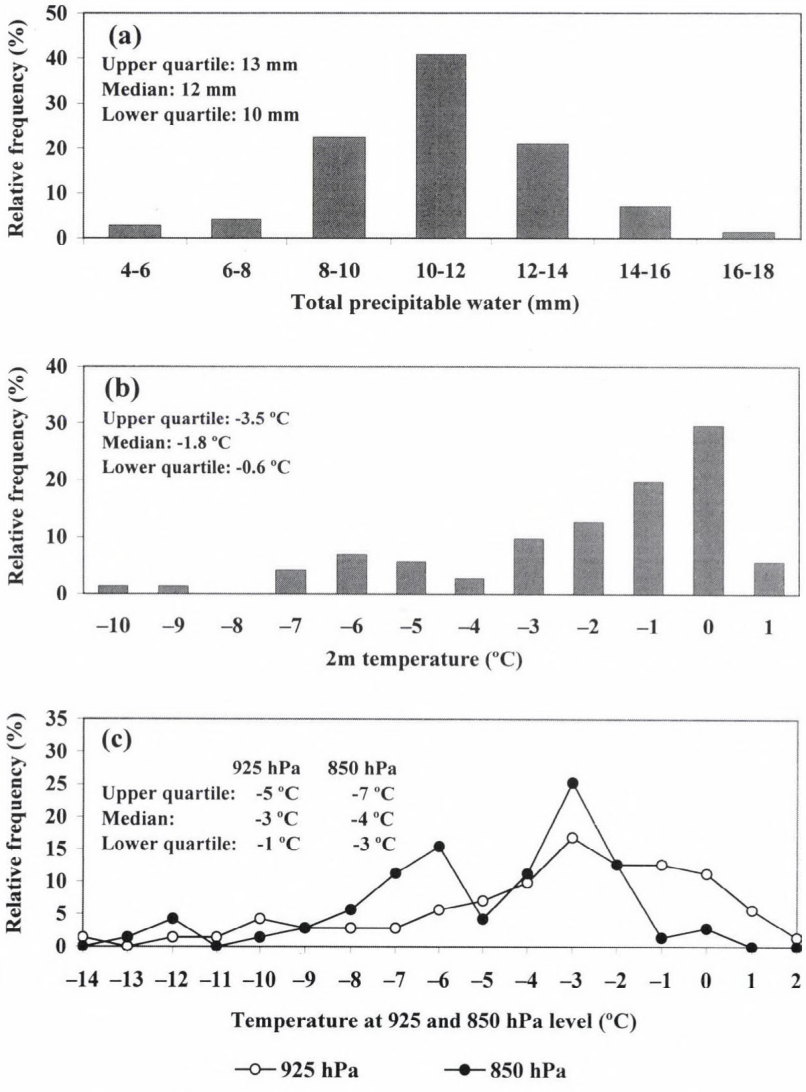

Fig. 3. Frequency distribution of the average total precipitable water (a), 2m temperature (b), and temperature at the 925 and 850 hPa level (c) for heavy snowfall events.

As far as 925 hPa level temperature is concerned, the highest average value reached +2 °C, accompanied by 0 °C at 850 hPa and +0.5 °C at 2 m, in a situation, when Hungary was located in the forward side of a cyclone under the influence of a strong warm advection. The coldest case had an average temperature of –14 °C at the 925 hPa level (–10 °C at 2 m). Median has been determined as –3 °C, while the average of all cases was –3.5 °C. The second half of the investigated period has turned out to be 0.5 °C colder than the first 25 years (*Table 2*). In case of all investigated temperature characteristics, January has the lowest average value, followed by February, December, November, and March.

4. Conclusion

In this study, characteristics of heavy snowfall events have been determined using a comprehensive database of SYNOP reports and analysis fields for a period of 50 years for Budapest. Cases of continuous snowfall producing a snow cover increase exceeding 8 cm have been selected, and several characteristics, including average intensity, snow depth increase, total precipitable water, etc., have been calculated for each case valid for the whole duration of the event. Investigation of the distribution and other statistical features of these characteristics has led to many valuable results.

It has been shown that on average, a precipitation amount of 1 mm corresponds to 1 cm of snow in November, December, and March, and to 1.5 cm in January and February. According to our research, the possible duration of heavy snowfall events with continuous precipitation in Budapest covers a wide time interval ranging from 3 hours up to more than 2 days. Also, snowfall intensity can vary considerably between 0.2 and 3.3 cm/hour, and the snow depth increase can reach almost 40 cm. In winter months like January, weather systems with lower mean sea level pressure over Central Europe can also lead to heavy snowfall events, while in November or March, average MSLP during HSEs is much higher, showing that the vicinity of a strong anticyclone is mostly necessary for heavy snowfall in these months.

The distribution of the investigated characteristics showed large variability from nearly exponential to symmetric, and it is negatively or positively skewed. Using the created empirical density functions, it is possible to estimate the probability of different values of the characteristics based on the long period of 50 years, which is essential when investigating rare meteorological events with a relative frequency of less than 1%, like in our case. The bimodality of the distribution found in case of some of the

characteristics (most significant for the temperature at the 850 hPa level) is also interesting.

The length of the investigated period makes it possible to look for potential signs of climate change by comparing the first and second half of the period. Interestingly, with most of the characteristics, there is only a slight change, pointing to the high stability of the climate system in terms of heavy snowfall events in Budapest. Comparing the two 25-year periods, the number of cases has increased only by 1 (from 35 to 36). In the frequency distribution of heavy snowfall events within the winter period itself, however, we have experienced very significant changes with the average number of HSEs, dropping to 50% in January, while increasing by 125% in November. As a result of this very significant modification, the frequency distribution of HSEs within the winter period has been completely rearranged, which might be a possible sign of climate change as well.

In Part II, results connected with the synoptic classification of heavy snowfall events will be presented. The dependency of HSEs' characteristics on their type will be investigated as well, allowing an even more efficient use of our results in operational weather forecasting.

Acknowledgements—The authors are grateful for the possibility of using NCEP Reanalysis data provided by the NOAA-CIRES ESRL/PSD Climate Diagnostics branch, Boulder, Colorado, USA, from their web site at http://www.cdc.noaa.gov.

References

Böhm, R., 1975: Lufttemperaturen bei Schneefall von größerer Ergiebigkeit in Wien. *Wetter und Leben 27*, 133-137.

Goree, P.A. and *Younkin, R.J.*, 1966: Synoptic climatology of heavy snowfall over the central and eastern United States. *Mon. Weather Rev. 94*, 663-668.

Gray, D.M. and *Male, D.H.*, 1981: *Handbook of Snow: Principles, Process, Management and Use*. Pergamon Press, Oxford.

McNulty, R.P., 1991: *Heavy Snow*. DOC/NOAA/NWS Training Center, Kansas City, MO.

Mote, T.L., Gamble, D.W., Underwood, S.J., and *Benthley, M.L.*, 1997: Synoptic-scale features common to heavy snowstorms in the southeast United States. *Weather Forecast. 12*, 5-22.

Schalko, M., 1949: *Grossschneefälle in Österreich*. Ph.D. Dissertation, Univ. Wien.

Spreitzhofer, G., 1999a: Spatial, temporal and intensity characteristics of heavy snowfall events over Austria. *Theor. Appl. Climatol. 62*, 209-219.

Spreitzhofer, G., 1999b: Synoptic classification of severe snowstorms over Austria. *Meteorol. Z. N.F. 8*, 3-15.

Wild, R., O'Hare, G., and *Wilby, R.*, 1996: A historical record of blizzards/major snow events in the British Isles, 1880-1989. *Weather 51*, 81-90.

Younkin, R.J., 1968: Circulation patterns associated with heavy snowfall over the United States. *Mon. Weather Rev. 96*, 851-853.

IDŐJÁRÁS

Quarterly Journal of the Hungarian Meteorological Service
Vol. 110, No. 1, January–March 2006, pp. 15–33

Regulatory modeling in Hungary — the AERMOD model. Part II. Sensitivity of the model and case studies

Roland Steib

Hungarian Meteorological Service
P.O. Box 39, H-1675 Budapest, Hungary; E-mail: steib.r@met.hu

(Manuscript received in final form February 24, 2006)

Abstract—This paper presents the sensitivity of a second-generation local-scale dispersion model, called AERMOD, which was adapted at the Hungarian Meteorological Service (HMS) in 2003. AERMOD was designed to introduce current planetary boundary layer concepts into regulatory dispersion models. In this paper the calculation of the most important planetary boundary layer parameters for dispersion calculations are described. The character of the boundary layer is represented with some case studies. We especially wanted to examine, what kind of meteorological parameters can result in high, short time average (1-hour) concentrations in the modeling domain. Finally, we also made a sensitivity analysis study of the newly implemented dry and wet deposition algorithms.

Key-words: regulatory modeling, local-scale dispersion model, planetary boundary layer, sensitivity analysis, concentration values, dry deposition, wet deposition

1. Introduction

In Part I of this study (*Steib* and *Labancz*, 2005) we presented a description of the AERMOD model and its application at the Hungarian Meteorological Service. A comparison between AERMOD and the formal dispersion model, called TRANSMISSION 1.0 (*Szepesi et al.*, 1995) was made. We found that the concentration distribution over flat terrain can differ significantly from the concentration distribution over elevated terrain when using the AERMOD model.

In Part II we explore the sensitivity of the model to various input and boundary layer parameters. We examine the relationship between high, peak (1-hour) concentration values at a receptor point in the modeling domain (with flat and elevated terrain) and the meteorological, surface, and boundary layer parameters.

During the summer of 2005, we have been changing our meteorological database used by the AERMOD model, in order to make calculations with the newly implemented deposition algorithms. Some sensitivity analysis studies were made to the input parameters of the deposition algorithms with the newest model version 04300, and the results are presented in this paper. The dry and wet deposition algorithms of AERMOD were originally released with version 03273, and they were modified with version 04079 and 04300.

2. *Basic algorithms in the AERMOD modeling system*

2.1 Planetary boundary layer algorithms in AERMET

As mentioned in Part I, the basic purpose of AERMET is to use meteorological measurements, representative of the modeling domain, to compute certain boundary layer parameters used in estimating profiles of wind, turbulence, and temperature.

AERMET defines the stability of the PBL by the sign of the surface sensible heat flux, H, (convective for $H>0$ and stable for $H<0$). At the transition point from convective to stable conditions, the heat flux changes sign. This transition occurs when the solar elevation angle reaches a critical value ($\varphi = \varphi_{crit}$). This critical value can be given with the following equation:

$$\sin \varphi_{crit} = \frac{1}{990}\left[\frac{-c_1 T^6 + \sigma_{SB} T^4 - c_2 n}{(1 - r\{\varphi\})(1 - 0.75 n^{3.4})} + 30\right], \tag{1}$$

where c_1 and c_2 are constants, σ_{SB} is the Stefan-Boltzman constant, T is the dry bulb temperature, n is the sky cover (in tenths), and $r\{\varphi\}$ is the albedo, which depends on the solar elevation. It can be seen, that the critical solar elevation depends on the temperature, albedo, and sky cover. For clear and partly cloudy conditions, the transition from stable to convective conditions occurs when φ reaches approximately 13°, for overcast conditions φ_{crit} increases to about 23° (*Holstag* and *van Ulden*, 1983). We can draw the following inference from this. When the geographical latitude of the modeling place is higher than 44.5° (in the Northern Hemisphere) or lower than -44.5° (in the Southern Hemisphere), then the planetary boundary layer can be stable through the whole day in case of an overcast winter day.

In the convective boundary layer (CBL), AERMET computes the friction velocity, u_*, and the Monin-Obukhov length, L, with an iterative method, similar to that used in CTDMPLUS (*Perry*, 1992), since the friction velocity and the Monin-Obukhov length depend on each other. In the stable boundary layer (SBL), the friction velocity and the Monin-Obukhov length are calculated with a simple semi-empirical approach.

The mixing height (z_i) in the CBL depends on both mechanical and convective processes and is assumed to be the larger of the mechanical mixing height (z_{im}) and convective mixing height (z_{ic}). In the SBL, the mixing height results exclusively from mechanical turbulence, and therefore, it is identically equal to z_{im}. The same expression for calculating z_{im} is used in both the CBL and SBL. The mixing height, z_i, for the convective and stable boundary layers is, therefore, defined as follows

$$z_i = MAX[z_{ic}; z_{im}] \qquad \text{for } L<0 \text{ (CBL)},$$

$$z_i = z_{im} \qquad \text{for } L>0 \text{ (SBL)}. \tag{2}$$

The procedure to estimate z_{ic} is the following. If measurements of the convective boundary layer are not available, the convective mixing height (z_{ic}) is calculated with a simple one-dimensional energy balance model (*Carlson*, 1973) as modified by *Weil* and *Brower* (1983). This model uses the early morning potential temperature sounding and the time varying surface heat flux to calculate the time evolution of the convective boundary layer as

$$z_{ic}\theta\{z_{ic}\} - \int_0^{z_{ic}} \theta\{z\}dz = (1+2A)\int_0^t \frac{H\{t'\}}{\rho c_p} dt' , \tag{3}$$

where θ is the potential temperature, A is set equal to 0.2 from *Deardorff* (1980), ρ is the density of the air, c_p is the specific heat at constant pressure, and t is the hour after sunrise.

Fig. 1 represents the relationship between the sensible heat flux and convective mixing height during a 48-hour (May 03, 2005, 00 LST–May 04, 2005, 23 LST) time period. We chose this 2-day time period, because the weather was changing in this period. On the first day the weather was warm and sunny, but on the next day it was colder, cloudy, and also windy. If the sign of H is negative, then z_{ic} is zero. If H is positive (during convective conditions), z_{ic} increases continuously. At the transition point to stable conditions, z_{ic} suddenly falls back to zero.

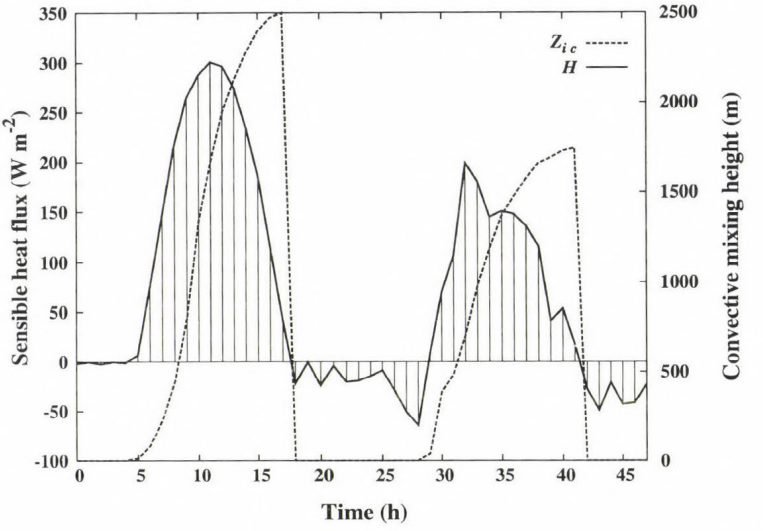

Fig. 1. Relationship between the sensible heat flux and convective mixing height during a 48-hour time period (May 03, 2005, 00 LST–May 04, 2005, 23 LST). Solid line represents the sensible heat flux (W m^{-2}), the dashed line represents the convective mixing height (m).

The procedure to estimate z_{im} is the following. *Venkatram* (1980) has showed that, in mid latitudes, the unsmoothed mechanical mixed layer height, z_{ie}, can be empirically represented as

$$z_{ie} = 2300 u_*^{3/2}. \tag{4}$$

The change of the friction velocity with time can cause sudden and unrealistic drops in the depth of the turbulent layer. Because of this effect, the current hour's smoothed mechanical mixed layer height is computed with the following equation

$$z_{im}\{t+\Delta t\} = z_{im}\{t\} e^{(-\Delta t/\tau)} + z_{ie}\{t+\Delta t\}\left[1 - e^{(-\Delta t/\tau)}\right], \tag{5}$$

where $z_{im}\{t\}$ is the previous hour's smoothed value, $\tau = z_{im} / \beta_\tau u_*$, which is the time scale, and $\beta_\tau = 2$. For computing the time scale, z_{im} is taken from the previous hour's estimate and u_* from the current hour. Eq. (5) shows that the current hour's smoothed mechanical mixing height is a combination of the

current hour's unsmoothed mechanical mixing height and the previous hour's smoothed mechanical mixing height. With this procedure, discontinuities in z_i are avoided. *Fig. 2* shows the relationship between the wind speed and the smoothed mechanical mixing height in the same 48-hour time period. It can be seen, that the character of the two curves is very similar. At the 19th hour, the smoothing effect is clearly visible. The wind speed falls suddenly, but the decrement of the smoothed mechanical mixing height is much more moderate. Eq. (2) results in that during stable conditions z_i is equal to z_{im}, during convective conditions z_i is the maximum of z_{im} or z_{ic}.

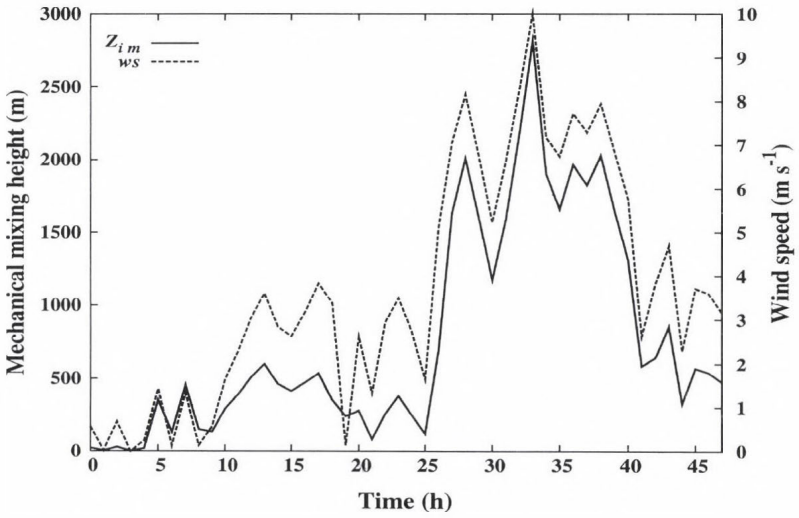

Fig. 2. Relationship between the wind speed and smoothed mechanical mixing height during a 48-hour time period (May 03, 2005, 00 LST–May 04, 2005, 23 LST). Solid line represents the smoothed mechanical mixing height (m), the dashed line represents the wind speed (m s^{-1}).

The behavior of this equation is made visible in *Fig. 3*, which shows the change of the PBL height in the same 48-hour time period. It can be clearly seen, that during the convective conditions of the first day, when the convective effects are stronger than the mechanical effects (sunny condition and low wind speed), z_i is equal to z_{ic} during the whole convective regime, but during the convective conditions of the second day, when the mechanical effects are stronger than the convective effects (cloudy condition and high wind speed), z_i is equal to z_{im} during the convective regime.

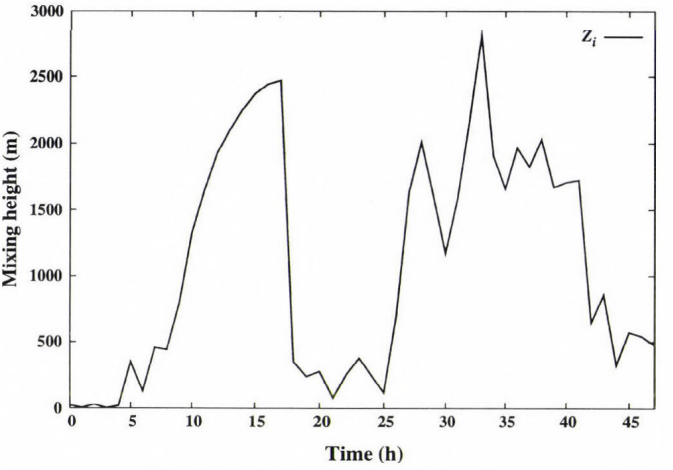

Fig. 3. The height of the planetary boundary layer during a 48-hour time period (May 03, 2005, 00 LST – May 04, 2005, 23 LST). Units: meters.

2.2 Dry and wet deposition algorithms in AERMOD

The dry and wet deposition algorithms in the AERMOD model were originally developed by the Argonne National Laboratory (ANL) for use in the ISC3 model. The model can handle five different deposition algorithms to calculate the deposition fluxes of a pollutant:

- dry deposition of particles (Method 1),
- dry deposition of particles (Method 2),
- gaseous dry deposition,
- wet deposition of particles,
- gaseous wet deposition.

2.2.1 Dry deposition algorithms

The dry deposition flux is calculated as the product of the concentration, χ_d, and a deposition velocity, V_d, computed at a reference height, z_r:

$$F_d = \chi_d \cdot V_d , \tag{6}$$

where F_d is the dry deposition flux (μg m^{-2} s^{-1}), χ_d is the concentration (μg m^{-3}), V_d is the deposition velocity (m s^{-1}), z_r is the deposition reference height (m) = z_0+1, and z_o is the surface roughness length for the application site (m).

Particle dry deposition

The dry deposition velocities of particles are simulated with a resistance scheme, in which the deposition velocity is determined based on the predominant particle size distribution. The model can use two methods to calculate the deposition velocities of particles.

Method 1

Method 1 is used when a significant fraction (greater than about 10 percent) of the total particulate mass has a diameter of 10 μm or larger. The particle size distribution must be known reasonably well in order to use Method 1. Eq. (6) is applied for each particle size category specified by the user, and the results are summed by the model. The particle deposition velocity for Method 1 is given as

$$V_{dp} = \frac{1}{R_a + R_p + R_a R_p V_g} + V_g, \tag{7}$$

where V_{dp} is the deposition velocity for particles (m s^{-1}), R_a is the aerodynamic resistance (s m^{-1}), R_p is the quasilaminar sublayer resistance (s m^{-1}), and V_g is the gravitational settling velocity for particles (m s^{-1}).

The aerodynamic resistance, R_a, is calculated as follows:

- for stable and neutral conditions (L>0),

$$R_a = \frac{1}{(ku_*)}\left[\ln\left(\frac{z_r}{z_0}\right) + \frac{5z_r}{L}\right], \tag{8a}$$

- for unstable conditions ($L<0$),

$$R_a = \frac{1}{(ku_*)}\left[\ln\frac{\left(\sqrt{1-16\frac{z_r}{L}}-1\right)\left(\sqrt{1-16\frac{z_0}{L}}+1\right)}{\left(\sqrt{1-16\frac{z_r}{L}}+1\right)\left(\sqrt{1-16\frac{z_0}{L}}-1\right)}\right], \tag{8b}$$

where k is the von Karman constant (0.4). For Method 1, the quasilaminar sublayer resistance, R_p, is calculated as follows

$$R_p = \frac{1}{(S_c^{-2/3} + 10^{-3/St})(1 + 0.24 w_*^2 / u_*^2) u_*}, \quad (9)$$

where Sc is the Schmidt number (dimensionless), St is the Stokes number (dimensionless), and w_* is the convective velocity scale (m s^{-1}). The gravitational settling velocity is calculated as follows

$$V_g = \frac{(\rho - \rho_{AIR}) g d_p^2 c_2}{18\mu} S_{CF}, \quad (10)$$

where V_g is gravitation settling velocity (m s^{-1}), ρ is the particle density input by user (g cm^{-3}), ρ_{AIR} is the air density ($\approx 1.2 \times 10^{-3}$ g cm^{-3}), g is the acceleration due to gravity (9.80616 m s^{-2}), d_p is the particle diameter (μm), S_{CF} is the slip correction factor (dimensionless), μ is the absolute viscosity of air ($\approx 1.81 \times 10^{-4}$ g cm^{-1} s^{-1}), and c_2 is the air units conversion constant (1.0×10^{-8} cm^2 μm^{-2}).

Method 2

Method 2 is used when the particle size distribution is not well known, and only a small fraction (less than 10 percent of the mass) of the particles has a diameter of 10 μm or larger. The deposition velocity for Method 2 is given as the weighted average of the deposition velocity for particles in the fine mode (i.e., less than 2.5 μm in diameter) and the deposition velocity for the coarse mode (i.e., greater than 2.5 μm but less than 10 μm in diameter):

$$V_{dp} = f_p V_{dpf} + (1 - f_p) V_{dpc}, \quad (11)$$

where V_{dp} is the overall particle deposition velocity (m s^{-1}), f_p is the fraction of particulate substance in fine mode (smaller than 2.5 μm in diameter). V_{dpf} is the deposition velocity (m s^{-1}) of fine particulate substance, calculated from Eq. (7) with V_g set to zero as

$$V_{dpf} = \frac{1}{R_a + R_p}, \quad (12)$$

V_{dpc} is the deposition velocity (m s^{-1}) of coarse particulate substance, calculated from Eq. (7) with V_g set to 0.002 m s^{-1} as

$$V_{dpc} = \frac{1}{R_a + R_p + 0.002 R_a R_p} + 0.002 . \quad (13)$$

For Method 2, the aerodynamic resistance is calculated using Eq. (8), and the quasilaminar sublayer resistance, R_p, is calculated with parameterizations based on observations of sulfate dry deposition:

- for stable and neutral conditions ($L > 0$)

$$R_p = \frac{500}{u_*}, \quad (14a)$$

- for unstable conditions ($L < 0$)

$$R_p = \frac{500}{u_* \left(1 - \frac{300}{L}\right)}. \quad (14b)$$

Gaseous dry deposition

For dry deposition of gases, the deposition velocity is given as

$$V_{dg} = \frac{1}{R_a + R_b + R_c}, \quad (15)$$

where V_{dg} is the deposition velocity for gases (m s^{-1}), R_b is the quasilaminar resistance for bulk surface (s m^{-1}), and R_c is the bulk surface resistance (s m^{-1}). The aerodynamic resistance, R_a, for gases is calculated the same way as for particles, using Eq. (8), except that a lower limit of 1000 s m^{-1} is applied to R_a. The quasilaminar sublayer resistance for bulk surface, R_b, is calculated as follows

$$R_b = \frac{2.2}{(k u_*)} \left(\frac{\upsilon}{D_a}\right)^{2/3}, \quad (16)$$

where D_a is the diffusivity of modeled gas in the air (m^2 s^{-1}) and υ is the kinematic viscosity of air. The bulk surface resistance is calculated as follows

$$R_c = \frac{1}{\left[\frac{LAI_r}{R_s + R_m} + \frac{LAI_r}{R_{cut}} + \frac{1}{R_{ac} + R_g}\right]}, \quad (17)$$

where LAI_r is the relative leaf area index (dimensionless), R_s is the canopy stomatal resistance (s m^{-1}), R_m is the canopy mesophyll resistance (s m^{-1}), R_{cut} is the canopy cuticular resistance (s m^{-1}), R_{ac} is the aerodynamic resistance in the vegetative canopy (s m^{-1}), and R_g is the resistance to uptake at the ground (s m^{-1}).

2.2.2 Wet deposition algorithms

The wet deposition flux is calculated on an hourly basis, and summed to obtain the total flux for the user-specified period. The default output units for wet deposition flux are g m^{-2}.

Particle wet deposition

The wet deposition flux for particulate substances is calculated from the particle-phase washout coefficient as follows

$$F_{wp} = 10^{-3} \rho_p W_p r, \quad (18)$$

where F_{wp} is the flux of particulate matter by wet deposition (μg m^{-2} hr^{-1}), ρ_p is the column average concentration of particulate in air (μg m^{-3}), W_p is the particle washout coefficient (dimensionless), and r is the water or water equivalent precipitation rate (mm hr^{-1}). The particle washout coefficient, W_p, is calculated as follows

$$W_p = \frac{3 z_p E}{2 D_m}, \quad (19)$$

where E is the collision efficiency (dimensionless), D_m is the mean diameter of raindrop (m) = $r^{0.232}/905.5$ with r in mm hr^{-1}, and z_p is the height of the top of plume or mixing height, whichever is greater (m). It is assumed that the washout coefficient, W_p, and therefore, the wet deposition flux, F_{wp}, is the same for frozen precipitation as for liquid precipitation. The collision efficiency is calculated after *Slinn* (1984) and *Seinfeld* and *Pandis* (1998).

Gaseous wet deposition

The wet deposition flux for gases is calculated as follows

$$F_{wg} = 10^6 C_l M_w r , \tag{20}$$

where F_{wg} is the flux of gaseous pollutants by wet deposition (μg m^{-2} hr^{-1}), C_l is the concentration of pollutant in the liquid phase (moles $liter^{-1}$), and M_w is the molecular weight of pollutant (grams $mole^{-1}$).

3. Results of the sensitivity analysis

3.1 Case studies of the planetary boundary layer

We made several test runs to examine the planetary boundary layer structure and the behavior of several meteorological and surface parameters. We especially examined the cases, when the short time (1-hour) averaging period concentration values were high in the modeling domain. This sensitivity analysis was made with the usage of flat and elevated terrains. In every model run the same source parameters were used as in Part I (*Steib* and *Labancz*, 2005), and the modeling domain was also the same.

3.1.1 Flat terrain

The maximum 50 1-hour average concentration values of NO_x were selected in the first 8 months of 2005. The highest 1-hour concentration was 22.28 μg m^{-3}, while the 50th highest was 14.36 μg m^{-3} in the modeling domain. We found that in 43 of 50 cases the maximum 1-hour concentration occurred during CBL and only in 7 of 50 cases during the SBL.

The 43 cases of the CBL could be divided into two major groups. The wind direction was parted to 16 sectors, and each of these sectors represents a unique group. The first group involved 10 cases, when the wind blew from west-southwest (236.25°–258.75°), the wind speed was low (1.0–1.2 m s^{-1}), and the surface roughness length was between 0.061 and 0.139 meters. The second group involved 15 cases, when the wind blew from the north (348.75°–11.25°), the wind speed was medium (2.9–6.6 m s^{-1}), and the surface roughness length was between 1.128 and 1.339 meters. The other 18 cases could be ordered in the other 14 groups. It should be mentioned, that the examined source (stack) is lying at the south border of the city of Pécs. The model

always uses the roughness length, which is characteristic of the area from where the wind blows, so it is not surprising that if the wind blows from the north (wind blows from urban area), then the value of the surface roughness length is much higher than that of the case of southwesterly winds (wind blows from rural area). It is also interesting, that the maximum 5 1-hour average concentration values (22.28–17.5 μg m^{-3}) could be assigned to the first group. In case of the 5 highest 1-hour concentrations the wind direction was 239°–251°, the wind speed was 1–1.2 m s^{-1}, and the roughness length was 0.061 meters. It is very likely, that this is an optimal combination of the wind speed and roughness length to result in the highest concentration values in the surface receptor points during CBL.

In 4 of the 7 cases of the SBL the wind direction was northerly (348.75°–11.25°), the wind speed was relatively strong (7.7–8.9 m s^{-1}), and the roughness length was between 1.212 and 1.339 meters. It can be seen that in spite of the stable conditions, the depth of PBL was high, because of the strong wind and high roughness length. That could be the reason for the good mixing of the polluted matter in the boundary layer during stable conditions too, and for the high concentration values at the surface receptor points.

In *Fig. 4*, the relative frequency of the wind direction during the maximum 50 1-hour average concentration is shown, when flat terrain was used.

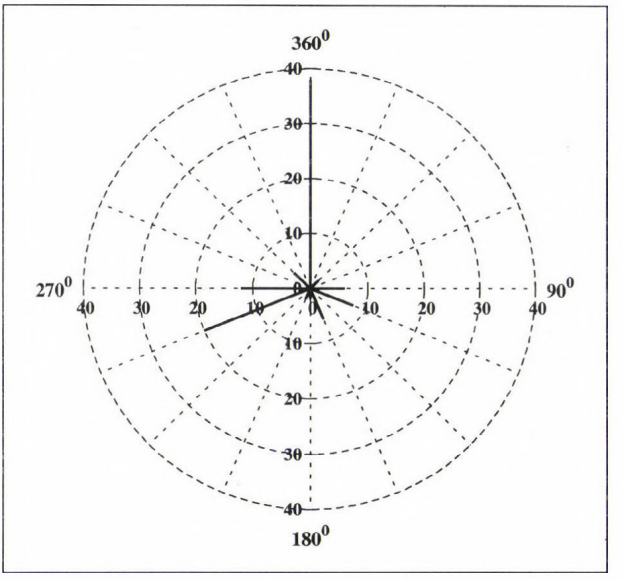

Fig. 4. Relative frequency of the wind direction (flat terrain) in case of the maximum 50 1-hour average concentration (%).

3.1.2 Elevated terrain

After the model run with elevated terrain, the maximum 50 1-hour average concentration values of NO_x were selected in the first 8 months of 2005. The first highest 1-hour concentration was 218.69 μg m^{-3}, and the 50th highest was 142.63 μg m^{-3}. We found that in all of the 50 cases the maximum 1-hour concentration occurred during SBL. In all cases the wind direction could be ordered into two groups. The first group involved 34 cases, when the wind direction was south-easterly (123.75°–146.25°), the second group involved 16 cases, when the wind direction was south-southeasterly (146.25°–168.75°). In all of the 50 cases the wind speed was low (0.5–1.7 m s^{-1}), and the surface roughness length was between 0.061 and 0.139 meters, except for two cases, when the height of the SBL was lower than or equal to 56 meters. The highest concentration values in the receptor points could be found, when the height of the stable boundary layer was lower than the height of the stack (80 m). At the 38th highest 1-hour concentration the SBL height was 165 meters, and at the 33rd it was even higher with 665 meters. It can be seen again, that the smoothing effect plays an important role. In both cases the wind direction changes to the opposite direction (from north-westerly to south-easterly) in short time, and this results in that the surface roughness length also decreases from about 0.906 meters to 0.061 meters. The wind speed also falls from 4 m s^{-1} to 1 m s^{-1} within a short time. The decrement of the wind speed and roughness length results in a sudden drop in the unsmoothed mechanical mixed layer height (z_{ie}), but the smoothing effect does not allow a sudden decrement of the current hour's smoothed mechanical mixed layer height (z_{im}). It is interesting to mention, that in case of the maximum 14 1-hour average concentration values (218.69–177.62 μg m^{-3}), the elevation over sea level of the receptor points with the highest 1-hour concentration values was the following: 299, 329, 334, and 338 meters. The elevation of the stack base over sea level was 150 m, so the highest concentration values were found 150–190 m above the stack base and 70–110 m above the stack top, consequently the following conclusions could be drawn. In case of modeling with elevated terrain, the highest concentration values could be found in those receptor points, which were at the height of the plume mass center.

In *Fig. 5*, the relative frequency of the wind direction during the maximum 50 1-hour average concentration is shown when elevated terrain was used. Although the same source parameters were used in case of flat and elevated terrain, the difference between the concentration values is significant. The concentration values by elevated terrain are about 10 times higher than those by flat terrain. These test runs made it clear again, that the model is the most sensitive to the terrain height of the modeling domain (also shown in Part I).

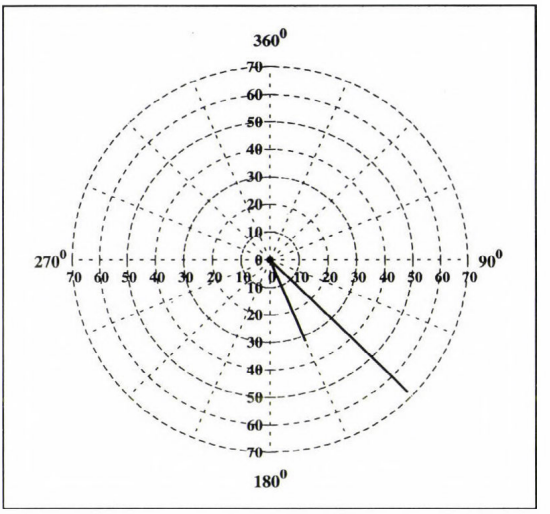

Fig. 5. Relative frequency of the wind direction (elevated terrain) in case of the maximum 50 1-hour average concentrations (%).

3.2 Case studies of the dry and wet deposition algorithms

In the sensitivity analysis to the input parameters of the dry and wet deposition algorithms, the same meteorological file was used as mentioned above (hourly meteorological data of the city Pécs, from the first 8 months of 2005). In this study all deposition fluxes were calculated on an hourly basis, and summed to obtain the total fluxes of this 8-month period, so the default output units for deposition fluxes are g m^{-2} for this 8-month time period.

3.2.1 Particle deposition flux

In our sensitivity studies the sensitivity of the particle deposition algorithms were examined based on Method 2. When using Method 2, the user must give two inputs to run the model: the mean particle diameter and the fine mass fraction of the particle. The value of the fine mass fraction can vary between 0 and 1, and the dimension of mean particle diameter must be μm.

In all of our sensitivity tests to particle deposition, we used flat terrain and a 1-dimensional polar coordinate system (only the y-coordinate changes between 100 and 20,000 m on north of the source) with the following source parameters:

- one point source (stack),
- type of pollutant: chromium,

- emission rate: 10 g s^{-1},
- release height above ground: 35 m,
- stack gas exit temperature: 400 K,
- stack gas exit velocity: 10 m s^{-1},
- stack inside diameter: 2.5 m.

In *Fig. 6*, the relationship between the period-averaged (8 months) surface concentration, the period-summed (8 months) dry and wet deposition fluxes is shown. It can be seen in this figure, that the structure of the concentration curve and dry deposition curve is very similar. The curve of the period-average concentration has its maximum place at 700 meters from the source, and the period-summed dry deposition curve at 600 meters. The character of the period-summed wet deposition curve is much more different. The highest wet deposition values can be found directly at the source, and it decreases rapidly as the distance from the source increases. The behavior of the dry and wet deposition curves is not surprising. The dry deposition depends on the concentration value, in consequence the character of the dry deposition curve must be similar to the character of the concentration curve. In case of wet deposition, the particles reach the ground with the falling raindrops, so the particle is able to reach the ground in a very short time. The highest column average concentration of airborne particles can be found directly at the stack exit, so we could detect the highest wet deposition values at the nearest receptor point to the source.

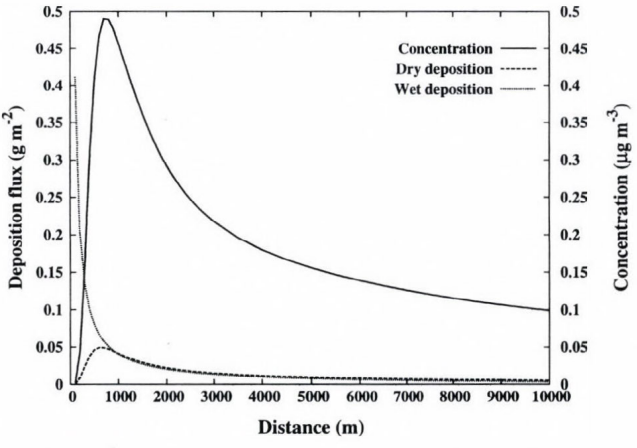

Fig. 6. Relationship between the period-averaged surface concentration, and the period-summed dry and wet deposition fluxes. Solid line represents the period averaged concentration (μg m^{-3}), dashed line represents the period dry deposition flux (g m^{-2}), and the dot line represents the wet deposition flux (g m^{-2}).

We also examined, how the change of the two input parameters (mean particle diameter and fine mass fraction) for Method 2 influences the dry and wet deposition fluxes. *Fig. 7* shows that only the dry deposition flux is dependent on the fine mass fraction. In the test runs the value of the fine mass fraction was changed from 0 to 1 with an increment of 0.1. In all cases a mean particle diameter of 2.5 μm was used. The figure shows that during the increment of the fine mass fraction, the dry deposition flux decreases linearly and the wet deposition flux remains constant. The conclusion is that the particle size distribution does not influence the wet deposition flux.

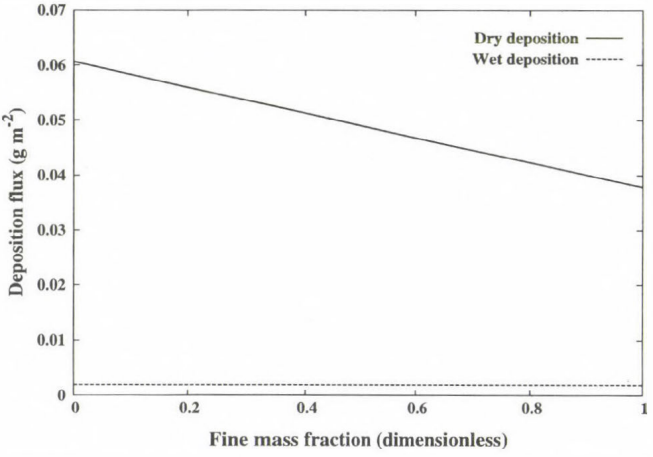

Fig. 7. Change of the dry and wet deposition fluxes as a function of the fine mass fraction. Solid line represents the dry deposition flux (g m^{-2}). Dashed line represents the wet deposition flux (g m^{-2}).

Fig. 8 represents the relationship between the mean particle diameter and deposition fluxes. In this case we can recognize the opposite effect of the deposition fluxes. In this model runs the value of the mean particle diameter was changed between 1 and 10 μm with a step of 1 μm. In all tests the fine mass fraction was 0.5. In this case the dry deposition flux remained nearly constant, but the wet deposition flux suddenly increased at the mean particle diameter of 3 μm. At a particle diameter of 1 μm, the value of the period-summed wet deposition flux was 0.00065 g m^{-2}, and the period-summed dry deposition flux was 0.04898 g m^{-2}. At 10 μm the wet deposition flux was 1.65558 g m^{-2} and the dry deposition flux was 0.04930 g m^{-2}. In this case the conclusion can be drawn, that the mean particle diameter hardly influences the dry deposition flux.

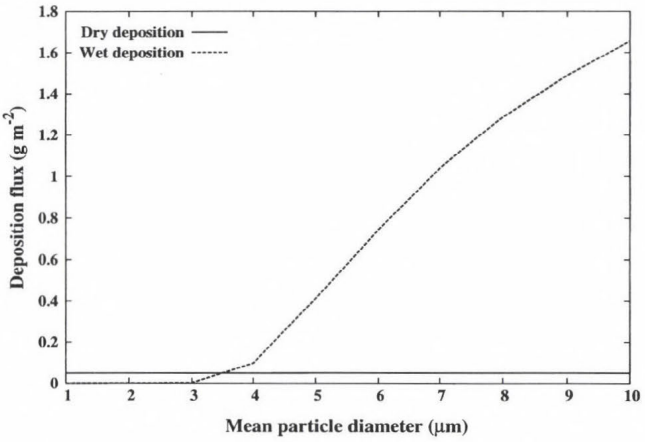

Fig. 8. Change of the dry and wet deposition fluxes as a function of the mean particle diameter. Solid line represents the dry deposition flux (g m^{-2}). Dashed line represents the wet deposition flux (g m^{-2}).

3.2.2 Gaseous deposition flux

When using gaseous deposition algorithms, the user must supply six mandatory inputs to run the model. These inputs are: diffusivity in air for the modeled pollutant (D_a), diffusivity in water for the modeled pollutant (D_w), cuticular resistance to uptake by lipids for individual leaves (*rcl*), Henry's Law constant (H), the Wesely seasonal categories, and the land use types. The gaseous deposition algorithms include some gas deposition resistance terms based on five seasonal categories (for each calendar month) and nine land use categories. The user should define land use categories for each of the 36 wind direction sectors.

Some model runs were made to examine the sensitivity of the gaseous deposition algorithms to the input parameters. The source parameters were the same as in the test runs of the particle deposition, except that the pollutant was benzene in every model run. We found that the particle deposition algorithms are more sensitive to the input parameters than the gaseous deposition algorithms. The diffusivity in air influences the dry deposition flux, while the diffusivity in water influences the wet deposition flux in the following way. When the diffusivity increases, the deposition fluxes also increase. The change of the cuticular resistance influences only the dry deposition flux. As the cuticular resistance increases, the dry deposition flux decreases. The Henry's Law constant influences the dry and also the wet deposition flux. As the

Henry's Law constant increases, the deposition fluxes decrease. The land use type influences only the dry deposition flux. *Table 1* shows the period-summed dry deposition flux at the 9 different land use categories. It can be clearly seen, that it is the wetness of the surface which most influences the dry deposition flux. In the case of a wet surface (bodies of water, wetland), the dry deposition flux is 1000–10000 times higher than in the case of a dry surface (urban area, desert).

Table 1. Dependence of the dry deposition flux on the land use type

Land use category	Description	Dry deposition flux (g/m^2)
1	Urban land, no vegetation	0.00000
2	Agricultural land	0.00091
3	Rangeland	0.00085
4	Forest	0.00089
5	Suburban areas, grassy	0.00079
6	Suburban areas, forested	0.00084
7	Bodies of water	0.30005
8	Barren land, mostly desert	0.00003
9	Non-forested wetland	0.05156

In our sensitivity analysis of the deposition algorithms, we examined only the model's sensitivity to the user defined deposition input parameters. The sensitivity of the deposition algorithms to the input meteorological parameters was not examined.

5. Conclusions

In this paper the basic planetary boundary layer algorithms of AERMET, and the deposition algorithms of AERMOD were presented. Then some test runs were made in order to examine the model's sensitivity to the input parameters of the boundary layer and deposition algorithms. It was not new that the wind direction, the wind speed, the surface roughness length, and the height of the planetary boundary layer are very important parameters when making concentration calculations, but it was more interesting to see, that the concentration distribution of the model was most sensitive to the terrain's elevation. It was also shown that the particle dry deposition flux (Method 2) is independent from the mean particle diameter, and the particle wet deposition

flux (Method 2) is independent from the fine mass fraction. Finally, the behavior of the gaseous deposition was presented. We found that the sensitivity of the gaseous dry deposition flux was higher than the sensitivity of the gaseous wet deposition flux to the input parameters.

The development of the AERMOD model is ongoing. We use the model mainly for regulatory purposes. We think that the sensitivity analysis of AERMOD in this paper was very useful, since our plan is to use the model also for other purposes in the future.

References

Carson, D.J., 1973: The development of a dry inversion-capped convectively unstable boundary layer. *Q. J. Roy. Meteor. Soc. 99*, 450-467.

Deardorff, J. W., 1980: Progress in Understanding Entrainment at the Top of a Mixed Layer.

Holtslag, A.A.M. and *van Ulden, A.P,* 1983: A simple scheme for daytime estimates for the surface fluxes from routine weather data. *J. Clim. Appl. Meteorol. 22*, 517-529.

Perry, S.G., 1992: CTDMPLUS: A dispersion model for sources in complex topography. Part I: Technical formulations. *J. Appl. Meteorol. 31*, 633-645.

Seinfeld, J.H. and *Pandis, S.N.*, 1998: *Atmospheric Chemistry and Physics*. John Wiley & Sons, Inc., New York, NY.

Slinn, W.G.N., 1984: Precipitation scavenging. In *Atmospheric Science and Power Production* (ed. *D. Randerson*). DOE/TIC-27601. U.S. Department of Energy, Washington, DC.

Steib, R., Labancz, K., 2005: Regulatory modeling in Hungary – the AERMOD model. Part I. Description and application. *Időjárás 109*, 157–172.

Szepesi, D.J., Fekete, K.E., Gyenes, L., 1995: Regulatory models for environmental impact assessment in Hungary. *Int. J. Environ. Pollut. 5*, 497-507.

Venkatram, A., 1980: Estimating the Monin-Obukhov length in the stable boundary layer for dispersion calculations. *Bound.-Lay. Meteorol. 19*, 481-485.

Weil, J.C. and *Brower, R.P.*, 1983: Estimating convective boundary layer parameters for diffusion applications. PPSP-MD-48, Maryland Power Plant Siting Program, Maryland Department of Natural Resources, Baltimore, MD, 45pp.

IDŐJÁRÁS

Quarterly Journal of the Hungarian Meteorological Service
Vol. 110, No. 1, January–March 2006, pp. 35–48

Comparing tendencies of some temperature related extreme indices on global and regional scales

Judit Bartholy and **Rita Pongrácz**

Department of Meteorology, Eötvös Loránd University
P.O. Box 32, H-1518 Budapest, Hungary
E-mails: bari@ludens.elte.hu, prita@elte.hu

(Manuscript received in final form February 6, 2006)

Abstract—Climate extreme indices are analyzed and compared for the Carpathian Basin for the 20th century based on the guidelines suggested by the joint WMO-CCl/CLIVAR Working Group on climate change detection. These climate extreme indices include the numbers of severe cold days, winter days, frost days, cold days, warm days, summer days, hot days, extremely hot days, cold nights, warm nights, the intra-annual extreme temperature range, the heat wave duration, the growing season length, etc. Therefore, daily maximum, minimum, and mean temperature observations are used in the present statistical analysis. Our results suggest that similarly to the global and continental trends, regional temperature of Central/Eastern Europe became warmer during the second half of the 20th century.

Key-words: extreme, climate index, daily maximum and minimum temperature, Carpathian Basin, Europe, trend analysis

1. Introduction

Since human and natural systems may be especially affected by changes of extreme climate events, the main objective of our research is to detect the possible changes of intensity and frequency of these extreme events. Previously, we presented the results of the analysis of extreme precipitation indices for the Carpathian Basin (*Bartholy* and *Pongrácz,* 2005a). This paper focuses on the extreme indices related to temperature.

According to the *IPCC* (2001), the detected shift in global mean temperature may result in more frequent extreme events. This is highlighted in the following example by *Schar et al.* (2004). They compared climate anomaly

time series based on past observations and model simulations for Switzerland. In the left panel of *Fig. 1*, summer precipitation and temperature anomalies of the last 140 years are presented. The right panel of *Fig. 1* shows the simulated anomalies for the 1961–1990 and 2071–2100 periods. Extreme heat waves occurred in Europe in summer, 2003. As the scatter plot diagrams highlight, the summer of 2003 was an extreme season compared to the past decades, while it can be considered as normal when looking at the simulated climate of Switzerland at the end of the 21st century.

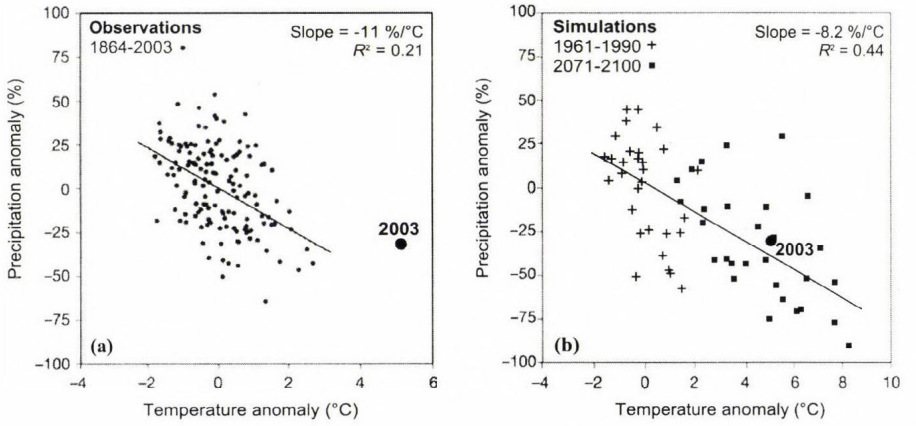

Fig. 1. Scatter plot diagrams of summer (JJA) mean temperature and precipitation anomalies for Northern Switzerland (*Schar et al.*, 2004), (a) on the base of observed data in 1864–2003, (b) on the base of simulated data for 1961–1990 (crosses), and for 2071–2100 (rectangles). Reference period is 1961–1990.

Giorgi and *Francisco* (2000) analyzed the future continental temperature and precipitation changes expected for the 21st century, based on model outputs of five main AOGCMs (Atmosphere-Ocean General Circulation Model). Global continental areas were divided into 23 regions, from which 2 cover the European continent, namely, (i) Northern Europe (NEU), and (ii) the Mediterranean region (MED). *Fig. 2* summarizes intensity, sign, and consistency of the GCM-based temperature changes for these two European regions. Expected changes in temperature conditions are presented in four small boxes for NEU and MED for 2071-2100. The upper and lower two boxes represent expected changes in winter (December-January-February), and in summer (June-July-August), respectively. Furthermore, results for the GG (greenhouse gas only case) and GS (greenhouse gas with increasing sulfate aerosol case) scenarios are shown in the left two boxes, and in the right two

boxes, respectively. The size of the "+" sign appearing in the small boxes indicate the intensity of temperature change compared to the baseperiod 1961–1990. Similarly, black and grey colors imply large (greater than 20%), and small (between 5% and 20%) average change, respectively. In case of model disagreement sign of inconsistency ("i") appears in the small box. In general, results of *Giorgi* and *Francisco* (2000) suggest that both winter and summer in Europe tend to be warmer than the present climate. Large increase of temperature can be expected in winter in Northern Europe and in summer in Southern Europe in case of the GS scenario. Estimations of the five main AOGCMs are inconsistent for NEU summers for the GG scenario.

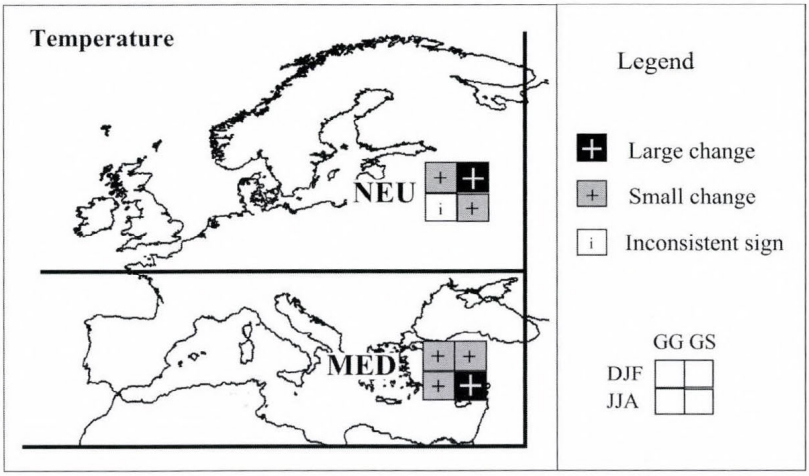

Fig. 2. Summary of temperature tendency analysis for Northern Europe (NEU) and the Mediterranean region (MED) for two seasons (winter and summer) and two climate scenarios (GG, GS), based on inter-model consistency analysis of *Giorgi* and *Francisco* (2000).

The *IPCC* (1995) concluded that changes in both the mean and extreme climate parameters may strongly affect human and natural systems. Furthermore, several research projects published results on the analysis of climate extremes on global or continental scales (e.g., *Easterling et al.,* 2000; *Peterson et al.,* 2002, etc.), and in order to strengthen the international cooperation, a Workshop on Indices and Indicators for Climate Extremes was held in Asheville (located in North Carolina, USA) in 1997. The required data sets for climate extreme analysis and the list of common climate extreme indices were compiled at this meeting (*Karl et al.,* 1999). Taking into account

the suggestions of the workshop, a joint WMO-CCl/CLIVAR Working Group formed on climate change detection in 1998 (*Frich et al.,* 2002). Results of their global and regional climate extreme analysis were provided for the *IPCC* (2001).

The next section of this paper summarizes and compares the results of the global (*Frich et al.,* 2002) and European (*Klein Tank* and *Können,* 2003) extreme analysis. Similar methodology has been applied to climate extremes of the Carpathian Basin. Section 3 discusses the continental (for Europe) and regional (for the Carpathian Basin) extreme tendencies. Finally, Section 4 concludes the main findings of this paper.

2. Climate extreme indices, comparison of global and European analysis

The CCl/CLIVAR task group on extreme indices compiled a global climate database containing daily precipitation, maximum, minimum, and mean temperature time series for the period 1946-1999. The main data sources include the national meteorological services, NOAA NCDC (*Peterson* and *Vose,* 1997), and the European Climate Assessment project (*Klein Tank et al.,* 2002b). All the datasets have been quality controlled and adjusted for inhomogeneities. Then, the following general criteria have been used for including an observation station: (i) from the entire 1946-1999 period, data must be available for at least 40 years, (ii) missing data cannot be more than 10%, (iii) missing data from each year cannot exceed 20%, (iv) in each year, more than 3 months consecutive missing values are not allowed.

Results of the global and European extreme climate analysis were published in *Frich et al.* (2002), and *Klein Tank* and *Können* (2003), respectively. In this section these results are summarized and compared for the global and continental scales. *Table 1* presents the main extreme indices that the CCl/CLIVAR task group identified and suggested for global climate extreme analysis. Besides the definition of each extreme index, the table indicates the scale (i.e., global, continental, regional) of application, as well. From the total 14 extreme temperature indicators, 5, 6, and 14 were used in the analysis for the world (*Frich et al.,* 2002), Europe (*Klein Tank* and *Können,* 2003), and the Carpathian Basin (*Bartholy* and *Pongrácz,* 2005b), respectively. For instance, *Figs. 3–5* present one of the climate extreme indices, namely, the change of the number of frost days ($T_{min} < 0°C$). Spatial distribution of global tendencies can be seen in *Fig. 3*, while the graph shown in *Fig. 4.* provides the temporal details of the global mean change of the number of frost days during the second half of the 20th century. Results of the similar analysis for Europe is presented in *Fig. 5.*

Table 1. Definition and indicator of extreme climate parameters

No.	Indicator (ECAD)	World (*Frich et al.*, 2002)	Europe (*Klein Tank* and *Können*, 2003)	Carpathian Basin (*Bartholy* and *Pongrácz*, 2005b)	Definition of the extreme temperature index	Unit
1	ETR	x		x	Intra-annual extreme temperature range (difference between the observed maximum and minimum temperatures, T_{max}–T_{min})	°C
2	GSL	x		x	Growing season length (start: when for more than 5 consecutive days $T>5$ °C, end: when for more than 5 consecutive days $T<5$°C)	day
3	HWDI	x		x	Heat wave duration index (for min. 5 consecutive days $T_{\max} = T^{N}_{\max} + 5$ °C, where $T^{N}_{\max}$ indicates the mean T_{max} for the baseperiod 1961–90)	day
4	Tx10		x	x	Cold days (percent of time when $T_{max}<10$th percentile of daily maximum temperature, based on the baseperiod 1961–90)	%
5	Tx90		x	x	Warm days (percent of time when $T_{max}>90$th percentile of daily maximum temperature, based on the baseperiod 1961–90)	%
6	Tn10		x	x	Cold nights (percent of time when $T_{min}<10$th percentile of daily minimum temperature, based on the baseperiod 1961–90)	%
7	Tn90	x	x	x	Warm nights (percent of time when $T_{min}>90$th percentile of daily minimum temperature, based on the baseperiod 1961–90)	%
8	FD	x	x	x	Number of frost days ($T_{min}<0$ °C)	day
9	SU		x	x	Number of summer days ($T_{max}>25$ °C)	day
10	Tx30GE			x	Number of hot days ($T_{max}\geq 30$ °C)	day
11	Tx35GE			x	Number of extremely hot days ($T_{max}\geq 35$ °C)	day
12	Tn20GT			x	Number of hot nights ($T_{min}>20$ °C)	day
13	Tx0LT			x	Number of winter days ($T_{max}<0$ °C)	day
14	Tn-10LT			x	Number of severe cold days ($T_{min}<-10$ °C)	day

Changes between the two subperiods of the second half of the century (1946–1975 and 1976–1999) have been determined during the analysis presented in *Frich et al.* (2002). The world map of *Fig. 3.* indicates both the sign of the change (gray and black circles for decreasing and increasing tendencies, respectively) and the magnitude of the change (applying 4 different circle sizes for different percentage intervals) at each station involved in the analysis. Stations with significant changes (at 95% level of confidence) in annual number of frost days are mapped with filled circles, while open circles indicate not significant changes. The large number of grey filled circles and very few black circles on the map suggest that the annual number of frost days decreased considerably between 1946 and 1999.

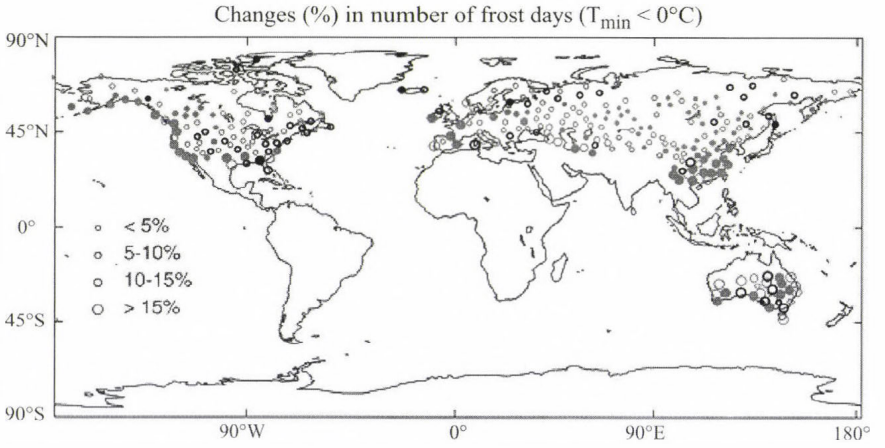

Fig. 3. Changes (%) in number of annual frost days in the second half of the 20th century. Filled circles are significant at the 95% level of confidence. Grey and black indicate negative and positive changes, respectively. Circle sizes represent the magnitude of change (source: *Frich et al.*, 2002).

Based on the available time series, annual global weighted mean anomalies have been calculated using the baseperiod of 1961–1990. *Fig. 4.* presents the annual value (in percentage) of the anomaly for the entire 1950–1999 period, and also, the fitted linear trend emphasizing the significant decreasing tendency. The figure includes a small graph (in its upper right part) indicating the total number of stations used for the analysis in each year. Except the beginning and the end of the period, about 300 stations provided valuable temperature data to determine the annual number of frost days.

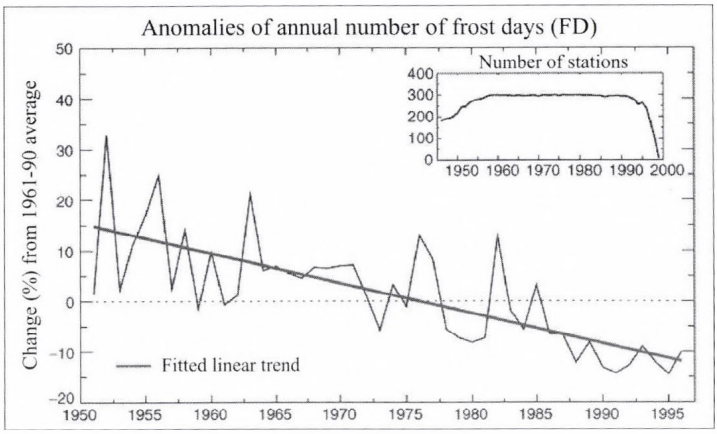

Fig. 4. Mean annual values of the number of frost days in percentage differences from the 1961–1990 weighted average values for the second half of the 20th century. The inserted graph represents the weighting factors (number of stations with valuable data) used in the linear regression analysis. The fitted linear trend is statistically significant at the 95% level of confidence (source: *Frich et al.*, 2002).

The European tendency analysis of the annual number of frost days is shown in *Fig. 5*, where the mean decadal changes of this extreme index is mapped for the stations with sufficient data for the 1946–1999 period. Open circles indicate not significant changes, while dark and grey filled circles indicate negative and positive trends, respectively. Similarly to the global analysis, significant negative tendency can be seen. Summarizing the above results of the two large scale analyses, annual number of frost days considerably decreased by the end of the 20th century.

Table 2 summarizes the tendencies of nine extreme indices for the global and continental scale climate analysis based on the papers of *Frich et al.* (2002), and *Klein Tank* and *Können* (2003), respectively. The comparison of these results is accomplished for the second half of the last century (1946–1999). Four indices (Tx10, Tx90, Tn10, and SU) are analyzed only on European scale. Increasing and decreasing trends are indicated with symbols „+" and „–", respectively. Two identical symbols represent large tendencies. Considerable spatial differences are emphasized using more than one type of symbols (e.g., –/+, ++/–, etc.), after identifying the main dominant trend, exceptions are listed in case of each extreme climate index. In general, global and European trends are similar, and refer to a warming climate tendency. Only a few small areas differ from these worldwide and continental dominant trends. For instance, in case of SU (summer days), Eastern Europe belongs to the exceptions. One of the aims of our research presented in this paper is to specify the trends on a finer spatial scale, and provide more details for the Carpathian Basin and Hungary.

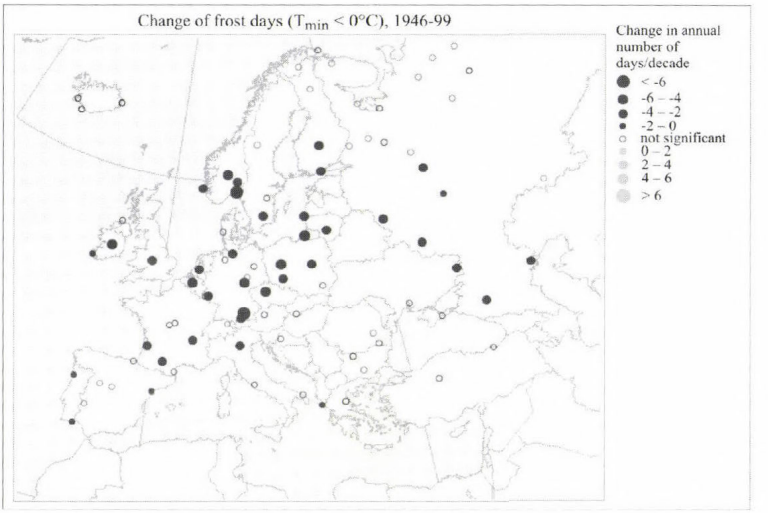

Fig. 5. Decadal trend in the annual number of frost days in Europe for the period 1946–1999. Circles are scaled according to the magnitude of the trend. Open circles indicate not significant changes, while dark and grey filled circles indicate negative and positive trends, respectively (source: *Klein Tank* and *Können,* 2003).

Table 2. Comparison of the tendencies of extreme climate indices, based on global (*Frich et al.,* 2002) and European (*European Climate Assessment & Dataset* project, *Klein Tank* and *Können*, 2003) extreme analysis for the period 1946–1999

No.	Extreme index	World (*Frich et al.,* 2002)	Europe (*Klein Tank* and *Können*, 2003)
1	ETR Intra-annual extreme temperature range	–	–
2	GSL Growing season length	+	+ + / – Positive tendency dominates except Iceland
3	HWDI Heat wave duration index	+ + / – Positive tendency dominates except SE-Asia and the eastern part of North-America	+
4	Tx10 Cold days	No analysis provided	+
5	Tx90 Warm days	No analysis provided	+ / – Positive tendency dominates except Iceland, Italy, and the Black Sea region
6	Tn10 Cold nights	No analysis provided	+ +
7	Tn90 Warm nights	+ +	+ + / – Positive tendency dominates except Iceland and the Black Sea region
8	FD Frost days	– –	– –
9	SU Summer days	No analysis provided	+ / – Positive tendency dominates except Eastern Europe

3. Analysis of extreme tempearture indices for the Carpathian Basin

In our analysis for the Carpathian Basin, daily temperature data from 13 meteorological stations are used. *Fig. 6* shows their geographical location. Minimum, maximum, and mean temperature time series of the 8 stations located outside Hungary are available from the ECAD site via the Internet (*Klein Tank,* 2003), while data from the 5 Hungarian stations are from the Data Archive of the Hungarian Meteorological Service. Two basic constraints are taken into account during the selection of the stations: (i) covering the area of the Carpathian Basin with the best spatial homogeneity and representing the main climatic subregions, (ii) time series without the least missing values during the 1961–2001 period. The analysis presented in this paper, is focused on the Carpathian Basin, however, two of the selected stations (Nis and Sarajevo) are outside this region. We included them in order to accomplish the analysis on a larger area.

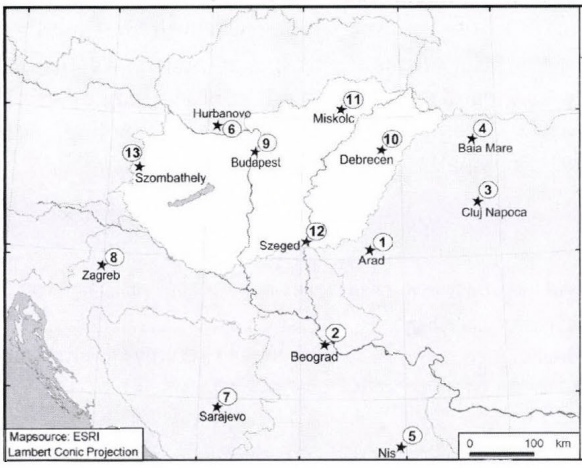

Station	Latitude (N)	Longitude (E)	Height above sea level (m)
1 Arad	46°08'	21°21'	117
2 Beograd	44°48'	20°28'	132
3 Cluj Napoca	46°47'	23°34'	410
4 Baia Mare	47°40'	23°30'	216
5 Nis	43°20'	21°54'	202
6 Hurbanovo	47°53'	18°12'	115
7 Sarajevo	52°30'	22°30'	211
8 Zagreb	45°49'	15°59'	157
9 Budapest	47°31'	19°02'	118
10 Debrecen	47°33'	21°37'	123
11 Miskolc	48°08'	20°48'	118
12 Szeged	46°15'	20°06'	82
13 Szombathely	47°15'	16°38'	218

Fig. 6. Geographical locations of the 13 meteorological stations used in the regional scale analysis for the Carpathian Basin. Note that Nis and Sarajevo do not belong to this region, but they were included in the analysis.

On the base of our previous study of time series of mean temperature and extreme temperature parameters, a strong warming tendency was detected from the middle of the 1970's (*Pongrácz* and *Bartholy*, 2000). Therefore, the entire 1961–2001 period has been separated into two subperiods, namely, 1961–1975 and 1976–2001. The tendency analysis has been accomplished for these subperiods. *Table 3* summarizes the increasing (+) and decreasing (-)

tendencies of the indices for the entire 41 years and for the two subperiods (15 and 26 years). Opposite sign of trend coefficients may indicate warming and cooling tendencies. For instance, negative coefficients of the number of cold days (Tx10) and positive coefficients of the number of hot days (Tx30GE) both indicate warming climate. Therefore, warming tendencies are shown in black boxes, while cooling tendencies in light grey. The trend coefficients of the index ETR (intra-annual extreme temperature range) are in white, since they do not imply either warming or cooling tendencies by themselves. Warming tendencies (in black) are dominant in the table. The regional climate of the Carpathian Basin tended to be warmer during the entire 41 years (except HWDI - heat wave duration index). In case of most of the extreme temperature indices, the three periods used in our analysis cannot be characterized by the same sign of trend coefficient. Only four extreme indices (Tn10 - cold nights, Tn-10LT - number of severe cold days, FD - number of frost days, Tn90 - warm nights) indicate warming tendency in the 1961-2001, 1961-1975, 1976-2001 periods. Based on the trend coefficients of HWDI, Tx90, SU, Tx30GE, Tx35GE, Tn20LT, the cooling tendencies until the middle of the 1970's is followed by a warming climate in the last quarter of the 20th century. Opposite tendency can be detected in case of two indices (Tx10, TxOLT) using regional scale average. However, these cooling trend coefficients of the last decades are small.

Table 3. Summary of the trend analysis of extreme temperature indices for the Carpathian Basin (warming and cooling trends are indicated by black and light grey color of the box, respectively)

No.	Extreme index	1961–2001	1961–1975	1976–2001
1	ETR: Intra-annual extreme temperature range	-	-	+
2	HWDI: Heat wave duration index	-	-	+
3	Tx10: Cold days	-	-	+
4	Tx90: Warm days	+	-	+
5	Tn10: Cold nights	-	-	-
6	Tn90: Warm nights	+	+	+
7	FD: Number of frost days	-	-	-
8	SU: Number of summer days	+	-	+
9	Tx30GE: Number of hot days	+	-	+
10	Tx35GE: Number of extremely hot days	+	-	+
11	Tn20GT: Number of hot nights	+	-	+
12	TxOLT: Number of winter days	-	-	+
13	Tn-10LT: Number of severe cold days	-	-	-

In this paper, detailed analysis is presented for the last quarter of the 20th century, when the largest changes occurred. Detailed tendency analysis of the indices Tn90 (warm nights) and Tx90 (warm days) are presented in *Fig. 7.* Trend maps for Europe and the Carpathian Basin are provided in the upper and middle panels, respectively, while the lower graphs show the regional mean index anomaly from the 1961–1990 average values for the Carpathian Basin. Circles represent decadal trend coefficients of the meteorological stations (using the baseperiod 1961–1990). Black and grey circles indicate increasing and decreasing tendencies, respectively, while circle size depends on the intensity of these positive or negative trends. In case of the regional mean, the fitted linear trends are clearly increasing between 1976 and 2001, in case of both indices. Also, no decreasing tendency can be identified in either map. The positive trend coefficients are significant at the 95% level of confidence.

The daily maximum temperature of summer is indicated by three extreme indices: (i) number of summer days (SU: $T_{max} > 25$ °C), (ii) number of hot days (Tx30GE: $T_{max} \geq 30$ °C), and (iii) number of extremely hot days (Tx35GE: $T_{max} \geq 35$ °C). As it can be seen from *Table 3,* increasing trend coefficients of these indices are detected during the entire 1961–2001 period and 1976–2001 subperiod, while they are decreasing in the 1961–1975 subperiod. *Fig. 8* presents the maps containing the increasing trend coefficients of extreme indices SU and Tx30GE in the Carpathian Basin in the last 26 years. Large positive trend coefficients dominate both maps, with more than 6 days per decade, in general. Tendency analysis map of the extreme index Tx35GE is not presented in this paper, since the frequency of this events is quite small, however, the trend coefficients are similar to those shown in case of SU and Tx30GE.

Similarly to *Fig. 7,* map with the trend coefficients of HWDI are shown in *Fig. 9.* As it can be seen on the maps, only significant increasing tendency of HWDI is detected in all of the stations in the last quarter of the 20th century. However, compared to the other indices, trend coefficients of more stations are not significant in Europe (left panel of the figure). The exact explanation is not known, but we can assume that the larger number of stations with insignificant tendency is related to the definition of this index. In the definition, the same 5 °C threshold is used in case of oceanic and continental climates, which may not be appropriate for all climates.

Based on the above figures, similarly to the global and European trends (*Frich et al.,* 2002; *Klein Tank et al.,* 2002a), analysis of the extreme temperature indices suggests that the regional climate of the Carpathian Basin tended to be warmer in the last 41 years.

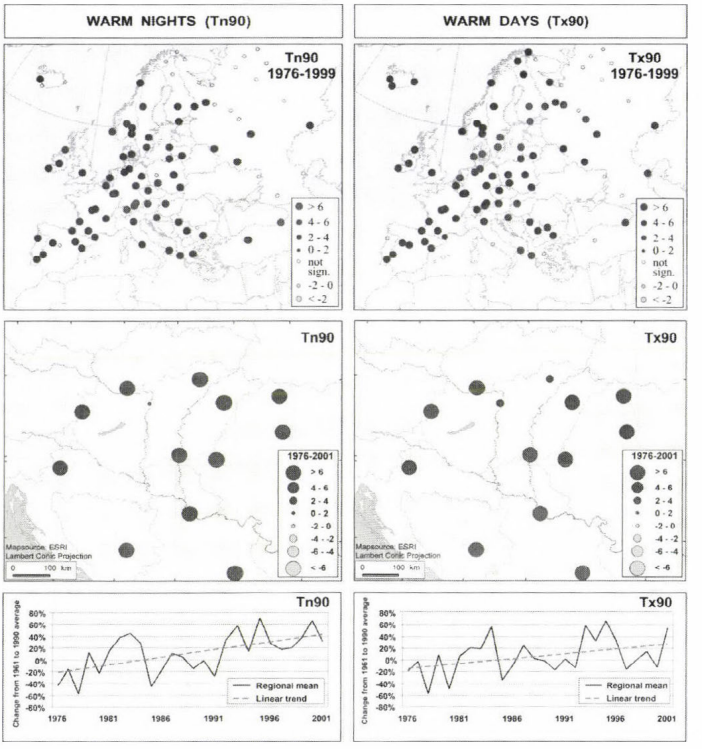

Fig. 7. Increasing tendency of warm nights (Tn90) and warm days (Tx90) in Europe and the Carpathian Basin during the last quarter of the 20th century. Trend coefficients of the Carpathian Basin greater than 0.4 in absolute value are significant at the 95% level of confidence.

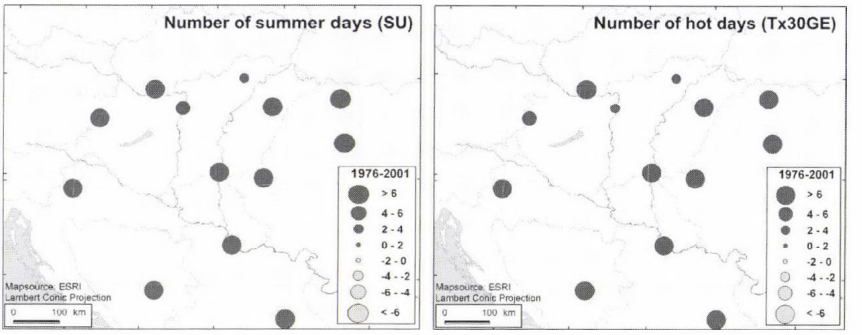

Fig. 8. Increasing tendency of the number of summer days (SU, $T_{max} > 25$ °C) and hot days (Tx30GE, $T_{max} \geq 30$ °C) in the Carpathian Basin during the last quarter of the 20th century. Trend coefficients greater than 0.4 in absolute value are significant at the 95% level of confidence.

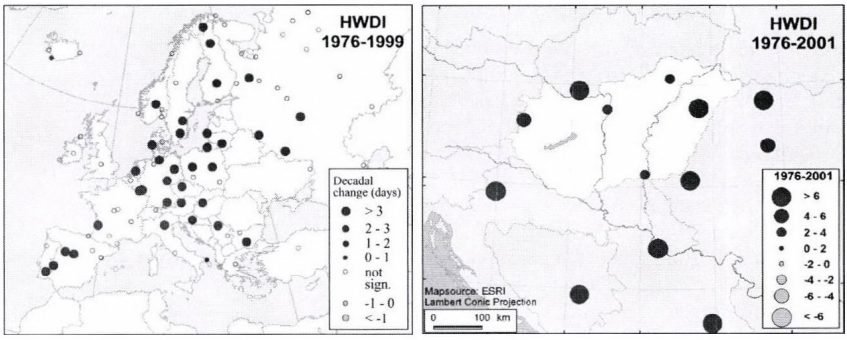

Fig. 9. Tendency of heat wave duration index (HWDI) in Europe and the Carpathian Basin during the last quarter of the 20th century. Trend coefficients of the Carpathian Basin greater than 0.4 in absolute value are significant at the 95% level of confidence.

4. Conclusions

The analysis of extreme temperature indices (according to the suggestions of the WMO-CCl/CLIVAR Working Group) are presented for the second half of the 20th century in this paper. Global and European trends of the extreme temperature indices are consistent with the global warming. As an example, the decreasing tendency of the number of frost days (FD) are presented on global (300 stations) and European (140 stations) scales. Based on the analysis of the extreme temperature indices for the Carpathian Basin, the following conclusions can be drawn.

- Significant warming tendencies are dominant during the entire 1961–2001 period.
- Most of the indices (e.g., HWDI, Tx90, SU, Tx30GE, Tx35GE, Tn20LT) show that the entire 41 years can be separated into a cooling period until the middle of the 1970's, and then a warming period in the last quarter of the 20th century.
- The largest trend coefficients (more than 6 days per decade) were detected in case of the following indices: Tn90, Tx90, SU, Tx30GE, HWDI.

Acknowledgements—Research leading to this paper has been supported by the Hungarian National Science Research Foundation (OTKA) under grants T-049824, T-034867, and T-038423, also by the CHIOTTO project of the European Union Nr. 5 program under grant EVK2-CT-2002/0163, the Hungarian National Research Development Program under grants NKFP-3A/0006/2002, NKFP-3A/082/2004, and NKFP-6/079/2005, and the VAHAVA project of the Hungarian Academy of Sciences and the Ministry of Environment and Water. ESRI software has been used to create maps.

References

Bartholy, J. and *Pongrácz, R.*, 2005a: Tendencies of extreme climate indices based on daily precipitation in the Carpathian Basin for the 20th century. *Időjárás 109*, 1-20.

Bartholy, J. and *Pongrácz, R.*, 2005b: Global and regional tendencies of extreme indices calculated on the base of daily temperature and precipitation for the 20th century (in Hungarian). *Agro-21. Füzetek*, 40, Magyar Tudományos Akadémia, Budapest, 70-93.

Easterling, D.R., Meehl, G.A., Parmesan, C., Chagnon, S.A., Karl, T., and *Mearns, L.O.*, 2000: Climate extremes: Observation, modelling and impacts. *Science 289*, 2068-2074.

Frich, P., Alexander, L.V., Della-Marta, P., Gleason, B., Haylock, M., Klein Tank, A.M.G., and *Peterson, T.*, 2002: Observed coherent changes in climatic extremes during the second half of the twentieth century. *Climate Res. 19*, 193-212.

Giorgi, F., and *Francisco, R.*, 2000: Evaluating uncertainties in the prediction of regional climate change. *Geophys. Res. Lett. 27*, 1295-1298.

IPCC, 2001: *Climate Change 2001: Third Assessment Report. The Scientific Basis*. Cambridge University Press, Cambridge, UK.

IPCC, 1995: *Climate Change 1995: The Science of Climate Change. Contribution of Working Group I to the Second Assessment of the Intergovernmental Panel on Climate Change*. Cambridge University Press, Cambridge, UK.

Karl, T.R., Nicholls, N., and *Ghazi, A.*, 1999: Clivar/GCOS/WMO Workshop on Indices and Indicators for Climate Extremes Workshop Summary. *Climatic Change 42*, 3-7.

Klein Tank, A.M.G., 2003: *The European Climate Assessment and Dataset project*. http://www.knmi.nl/samenw/eca/index.html.

Klein Tank, A.M.G. and *Können, G.P.*, 2003: Trends in Indices of Daily Temperature and Precipitation Extremes in Europe, 1946-99. *J. Climate 16*, 3665-3680.

Klein Tank, A.M.G., Wijngaard, J.B., Können, G.P., Böhm, R., Demarée, G., Gocheva, A., Mileta, M., Pashiardis, S., Hejkrlik, L., Kern-Hansen, C., Heino, R., Bessemoulin, P., Müller-Westermeier, G., Tzanakou, M., Szalai, S., Pálsdóttir, T., Fitzgerald, D., Rubin, S., Capaldo, M., Maugeri, M., Leitass, A., Bukantis, A., Aberfeld, R., van Engelen, A.F.V., Forland, E., Mietus, M., Coelho, F., Mares, C., Razuvaev, V., Nieplova, E., Cegnar, T., Antonio López, J., Dahlström, B., Moberg, A., Kirchhofer, W., Ceylan, A., Pachaliuk, O., Alexander, L.V., and *Petrovic, P.*, 2002a: Daily dataset of 20th-century surface air temperature and precipitation series for the European Climate Assessment. *Int. J. Climatol. 22*, 1441-1453.

Klein Tank, A.M.G., Wijngaard, J.B., and *van Engelen, A.*, 2002b: *Climate of Europe; Assessment of observed daily temperature and precipitation extremes*. KNMI, De Bilt, the Netherlands, 36p.

Peterson, T.C. and *Vose, R.S.*, 1997: An overview of the global historical climatology network database. *B. Am. Meteorol. Soc. 78*, 2837-2849.

Peterson, T., Folland, C.K., Gruza, G., Hogg, W., Mokssit, A., and *Plummer, N.*, 2002: Report on the Activities of the Working Group on Climate Change Detection and Related Rapporteurs, 1998-2001. *World Meteorological Organisation Rep. WCDMP-47. WMO-TD 1071*. Geneva, Switzerland. 143p.

Pongrácz, R. and *Bartholy, J.*, 2000: Changing trends in climatic extremes in Hungary (in Hungarian). In *III. Erdő és Klíma Konferencia* (ed.: *A. Kircsi*). Kossuth Lajos Tudományegyetem, Debrecen, 38-44.

Schar, C., Vidale, P.L., Luthi, D., Frei, C., Haberli, C., Liniger, M.A., and *Appenzeller, C.*, 2004: The role of increasing temperature variability in European summer heatwaves. *Nature 427*, 332-336.

IDŐJÁRÁS

Quarterly Journal of the Hungarian Meteorological Service
Vol. 110, No. 1, January–March 2006, pp. 49–62

Effects of documented land use changes on the albedo of Eastern Hungary (1951–2000)

János Mika[1*], **Szilvia Horváth**[2**] and **László Makra**[2]

[1]*Hungarian Meteorological Service*
P. O. Box 38, H-1525, Budapest, Hungary;
E-mail: mika.j@met.hu

[2]*Department of Climatology and Landscape Ecology, University of Szeged*
P.O. Box 653, H-6701 Szeged, Hungary; E-mail: makra@geo.u-szeged.hu

(Manuscript received in final form February 20, 2006)

Abstract—Agricultural land use series are investigated in a plain catchment area of the river Tisza within Hungary, almost identically represented by six administrative counties. Each county, commonly covering 34,900 km^2, is characterized by high percentage (72–82%) of managed vegetation. Effects of the area coverage variations between the different plant species are computed for the period 1951–2000, by applying results of literature-based syntheses specified for Hungary. The latter studies estimate surface albedo values for the great majority of the plant species grown in the region. Product of the plant-specific albedo values and the relative area coverage results in monthly series of surface albedo. Furthermore, by using a radiation transfer model, these series are also used to simulate radiation balance series for the surface-atmosphere system. Two questions are investigated and positively answered: (i) Are there monotonous trends in the radiation balance? (ii) Are these changes comparable to the effects caused by other external forcing factors?

Key-words: land use, albedo, radiation balance, climate change, Hungary.

1. Introduction

Solar radiation absorbed by the global Earth-atmosphere system is about 235 W m^{-2} (e.g., *IPCC*, 2001, Chapter 1.2.1). Since the 19th century, the atmospheric CO_2 has been responsible for 1.5 W m^{-2} primary radiation change

* Corresponding author

** Present affiliation: Ministry of Environment and Water Management, Environmental Policy and Impact Assessment Department, Fő u. 44-50, 1027 Budapest, Hungary; E-mail: horvathszil@mail.kvvm.hu

at the top of the atmosphere *(IPCC*, 2001, Chapter 6*)*. At the same time, CH_4 is computed to be responsible for 0.55 W m^{-2}, N_2O for 0.2 W m^{-2}, and CFC gases together for 0.3 W m^{-2}. Consequently, total growth of the radiation balance is 2.5 W m^{-2}, which as medium estimation, is equivalent to 1.5 K global temperature increase. However, only 0.7 K warming is observed. This difference is explained by the decrease of ozone in the stratosphere (- 0.2 W m^{-2}) and by the anti-greenhouse effect caused by tropospheric aerosols (-1 – -2 W m^{-2}), together with the enormous heat capacity of the oceans.

Consequently, recent climate forcing considerations are based on calculations originating from about 1% change of the energy balance. This is a very little number compared either to measuring accuracy of most environmental physical variables, or to relative errors of model calculations. Hence, it is worth studying various other external factors and feedback mechanisms, which, in addition to greenhouse gases and aerosols, might influence the climate.

One set of the possible feedback mechanisms is connected to the vegetation. In global average, plant structure changes caused –0.2 W m^{-2} radiative forcing (*IPCC*, 2001). Role of plant cover has already been mentioned in the literature since the 1970's, when two possible ways of surface modification, namely overgrazing in the subtropics and devastation of rain forests were counted to be potential causes of the global climate change (*Charney et al.*, 1977; *Sagan et al*, 1979). Both changes express their effect on climate through the light reflecting capacity of the surface, i.e., its albedo.

The Sahel climate problem is investigated by some models (*Xue* and *Shukla*, 1993), and the possibility of vegetation feedbacks on paleo-climatic events are also considered (*de Noblet et al.*, 1996; *Texier et al.*, 1997). Physical sub-model of mosaic vegetation is incorporated in the GCMs already for about a decade (*Claussen*, 1994).

Concerning the problem in the given area, Hungary, three possible feedback mechanisms, connected to surface albedo modifications, were quantified by *Mika et al.* (1992), in relation to likely scenarios (*Mika*, 1988) pointing at warmer and drier climates parallel to global warming. These are the change in duration of the vegetation period, the less precipitation, and the adequate alterations in the managed vegetation, all induce an increase of the surface albedo. The sum of these feedbacks was assessed to be –0.7 W m^{-2}, presuming changes in vegetation cover due to regional consequences of the 0.5 K global warming in Hungary. This value is comparable to the radiative forcing of 100 ppm increase of the CO_2 concentration (*Mika et al.*, 1991).

The present study is aimed to analyze the effects of documented changes in the managed vegetation on the surface albedo and radiation balance of the

surface-atmosphere system above a selected region, delimited by hydrological considerations. The paper is structured as follows: Section 2 describes the methods of computation for surface albedo and shortwave radiation balance of the surface-atmosphere system, perturbed by the changes of vegetation. Section 3 introduces the investigated region in Eastern Hungary and the documented changes of vegetation during the 1951–2000 period. Section 4 presents the results of computed changes in the above two solar radiation components, which are also compared with the changes hypothetically caused by a few other factors. Validity and limitations of these computations are discussed in Section 5.

2. Albedo estimation methodology

2.1 Surface albedo

Surface albedo is influenced by the type and state of soils, species of plant cover, and its growing phase. In the course of preparing the albedo maps of Hungary, *Dávid* (1985) issued synthesis values of surface albedo. On the basis of temporal difference of growing phases, territory of Hungary was divided into two or three plant-specific regions, according to the temporal shifts in growing phases between the northern and southern parts of the country. *Dávid* established surface albedo values for these regions and groups of plants in ten days' resolution. Average monthly surface albedo of plants, most frequently cultivated in Hungary, are listed in *Table 1*, where Region 1 indicates southern part of Eastern Hungary, while Region 2 relates to its northern part. The two regions differ in their average climatic characteristics.

2.2 System albedo and radiation balance

Variations of albedo and radiation balance can be determined not only for the surface, but for the surface-atmosphere system, as well. This makes the comparison between the energy changes due to surface modification and the primary effects of other climate forcing factors possible. These forcing factors are, e.g., the atmospheric CO_2 concentration, solar constant, or volcanic aerosols, which are usually estimated at the top of the atmosphere.

For this aim, results of a former calculation (*Mika et al.*, 1993), made by the help of a radiative-convective model (*Práger* and *Kovács*, 1988), adapted after *Karol* and *Frolkis* (1984) was used, by freezing its convective adjustment and other feedback mechanisms. The model is horizontally averaged, with 16 levels of computation from 1000 hPa at the surface to 0.64 hPa at about 60 km altitude. The vertical resolution is 100 hPa in the troposphere.

Table 1. Average surface albedo of some plant species (source: *Dávid*, 1985). Region 1 and 2 correspond to the southern and northern parts of Eastern Hungary, respectively. (Monthly averages are shown for demonstration. The computations use the original 10-day specifications.)

Region	Surface albedo (%)						
	April	May	June	July	August	September	October
				wheat			
1.	18	20	23	23	21		
2.	18	20	21	23	21		
				barley			
1.	17	20	21	23	21		
2.	17	19	21	23	21		
				rye			
1.	18	20	21	23	20		
2.	18	19	21	23	20		
				maize			
1.		15	18	23	23	24	25
2.		15	17	20	23	23	25
				alfalfa			
1. & 2.	23	20	23	22	23	23	19
				potato			
1.	15	19	24	20	18	19	
2.	15	18	22	23	19	19	
				sugar beet			
1.	14	15	19	19	21	22	22
2.		14	18	19	20	22	22
				meadow and pasture			
1. & 2.	17	19	20	20	19	20	19
				forests (in leaf and conifers)			
1. & 2.	14	14	14	14	14	14	14

Broadband approximation, based on empirical transmission functions, is applied for 24 and 17 spectral intervals in the short- and longwave parts of the radiation spectrum, respectively. Longwave transmission functions are adapted from *Rozanov et al.* (1981). The δ-Eddington method is used for parallel computation of absorption and scattering. Optical thickness is calculated by the Curtis-Godson approximation. (For both latter approaches see, e.g., *Liou*, 1980).

Internal parameters and astronomical conditions of the model are defined for Budapest (47°26'N; 19°17'E). Cloud amounts of the different levels are taken from *Warren et al.* (1985), and a proportional vertical normalization is performed to obtain the total cloud coverage valid in the local climate. Low- and medium-level clouds are considered as blackbodies for longwave radiation. High-level cloudiness is characterized by 0.5 emissivity. The aerosol optical profile is adapted from *WMO* (1983) considering "continental background" aerosol.

By this model we determined, how surface albedo changes affect the shortwave energy balance, R_s, of the surface-atmosphere system. Connection between this term and the system albedo, α_s, is

$$\Delta R_s = -G_0 \cdot \Delta \alpha_s , \tag{1}$$

where G_0 is the solar energy reaching the top of the atmosphere.

According to computations with the above radiative model (*Mika et al.*, 1992), the dependence of the system albedo on the surface albedo, α, is nearly linear (*Fig. 1*)

$$\Delta \alpha_s = k \cdot \Delta \alpha . \tag{2}$$

One percent change of surface albedo involves k = 0.40–0.45 percent change in system albedo during the examined seven months. Deviation of k from 1.0 can be explained by the cloudiness and limited transparency of the atmosphere. The higher values of k characterize the summer period, when cloudiness is less and the optical path is shorter.

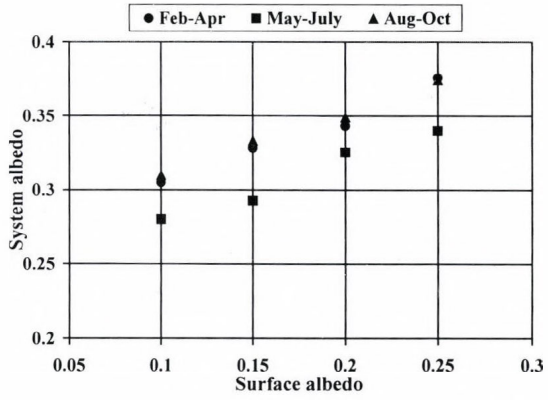

Fig. 1. Correlation between the surface albedo and the albedo of the surface-atmosphere system in different periods of the year, as computed by a radiation model for Hungary.

For the three "astronomical" seasons (February–April, May–July, and August–October), the radiative calculations yielded slightly different k values (k=0.406, 0.446, 0.400, respectively), from which the annual course can be approached by the following formula

$$k(h) = a_1 \cdot h^2 + a_2 \cdot h + a_3, \tag{3}$$

where h is the serial number of the months (February = 2, etc.). Substituting the three-monthly averages of these numbers into Eq. (3), the $a_1,\ldots,a_3$ coefficients and the monthly variation of $k(h)$ were calculated.

3. *Regional specification*

3.1 The selected region

The region, selected for the investigation, is the sub-catchment area of the river Tisza (*Fig. 2*) in the Hungarian plain, partly bordered by the administrative border of the country. This region of 35,700 km^2 was previously used for regional energy- and water balance modeling (*Mika et al.*, 1991, 1998).

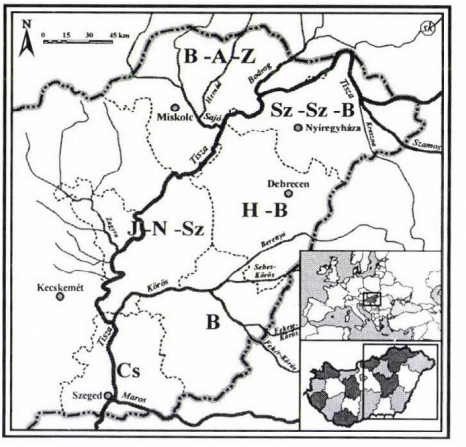

Fig. 2. The river Tisza sub-catchment in Eastern Hungary. The indicated administrative counties approximately cover this hydrological unit. Total area of the six counties is 34,900 km^2.

However, the land use data are officially published on a county by county basis (see in Section 3.2), hence this region should be approximated by administrative counties. Six of them, namely Borsod-Abaúj-Zemplén, Szabolcs-Szatmár-Bereg, Hajdú-Bihar, Jász-Nagykun-Szolnok, Békés, and Csongrád counties approximately cover the targeted hydrological region. More exactly, this 34,900 km^2 administrative area is the object of the investigations.

The Hungarian catchment area of the river Tisza exhibits the lowest altitude of about 100 m above the sea level, in the Carpathian Basin. This large

landscape has always been characterized by high proportionality of managed vegetation. Recently, 74% of the total administrative area is cultivated. The rest of the area, mainly the natural vegetation of the Hungarian Plain, represents the westernmost extension of this forest-steppe zone in Europe.

Soil formation factors here are favorable to the development of meadow alluvial and alluvial meadow soils along the rivers, solonetz in the center of the region and chernozem mostly in the southern part of the landscape. The latter mentioned chernozem is the most fertile kind of soils in Hungary.

As compared to the annual mean temperature (9.3–10.6 °C), the annual mean precipitation amount (500–600 mm per year) is far from the optimum.

3.2 Land use series

In this chapter it is briefly shown, how the sown area of the different plant species varied in the six examined counties during the period 1951–2000, according to the data in the annual reference books of the *Central Statistical Office* (1951–2000) and *Historical Statistical Contributions* (1971–79).

For easier interpretation, the plant species of the computations can be arranged into five groups:

- *cereals* – winter wheat, rye, barley, and rice;
- *fodder-plants* – maize, alfalfa, red clover, maize for silage, oat, and cattle-turnip;
- *food- and industrial plants* – sugar beet, tobacco, sunflower, potato, and fibre hemp;
- *vineyard and fruits*;
- *others*: forest, meadow, and pasture.

Total area of agricultural land use in the examined region shows a gradually decreasing tendency (*Fig. 3*). Considering the examined 1951–2000 period, the sown area of cereals and fodder-plants has decreased considerably, especially since the early 1990's. Tendencies of the sown area for food- and industrial plants varied from one county to the other, with no clear tendency in the whole region. Share of the sown area for vineyard and fruits is an order of magnitude smaller, than that of the other four groups of plants. Share of forest, meadow, and pasture in the six counties did slightly increase in 1951–2000, contrary to the other groups of plant species. These tendencies are also demonstrated in *Table 2* by selected five-year averages of the five groups of plant species.

Total share of the considered agricultural areas is the least in Hajdú-Bihar county (0.71) and the highest is in Csongrád and Jász-Nagykun-Szolnok (0.80). Altogether, 74% of the total area are involved in the investigation. For the rest of the area no changes are postulated.

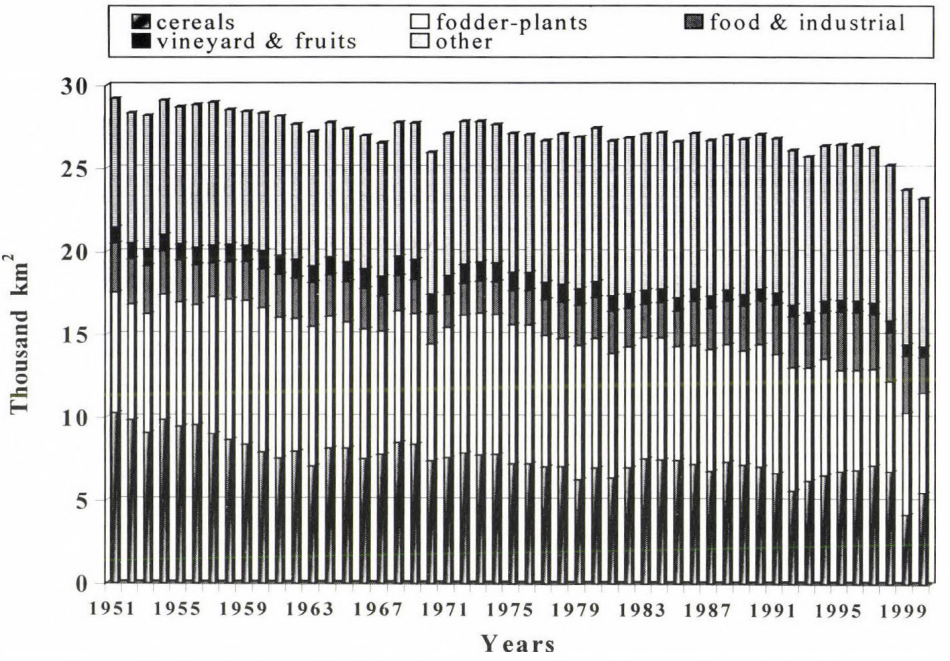

Fig. 3. The total cultivated area and its share among the main plant groups in the examined region, 1951–2000.

In computation of areal average albedo, however, variations of the total sown area are not considered, since the area-weighted sums will be normalized by this area, i.e., by the sum of the weights. Possible variations at the set-aside areas are not included in our estimations.

Table 2. Land use change tendencies in Eastern Hungary expressed in selected time periods (in thousands of km²)

Time period	Cereals	Fodder plants	Food & industrial	Vineyard & fruits	Forest, meadow, pasture	All land in use	Total area	Part of land in use (%)
1951–1954	9.76	7.25	2.80	9.76	7.90	28.68	34.90	**82.2**
1973–1978	7.35	8.22	2.09	10.97	8.44	27.20	34.90	**77.9**
1995–2000	6.22	5.90	3.16	6.81	9.22	25.18	34.90	**72.2**

3.3 Area weighting

The effect of any fluctuation or change in land use on some A quantity (in present study the surface albedo) is calculated in the following way. Suppose, that in a given t year each considered plant sort takes up $T^i(t)$ territory in the examined region. The sum of these kind of territories is in this case is

$$T_m(t) = \sum_i T^i(t), \quad i = 1, 2, \ldots \quad . \tag{4}$$

Introduction of the above mentioned land use is actually connected to this total $T_m(t)$ territory and, within this, to $T^i(t)$ share territories. Albedo selection and weighting is performed by areas of the original plant species, without any grouping.

Regional variation of the areal mean, $A_m(t)$, quantity is determined by the plant-specific $A_i(t)$ values, also depending on the vegetation phase, and by the $T^i(t)$ area of the different plant species (land use forms), as

$$A_m(t) = \frac{1}{T_m(t)} \sum_i T^i(t) \cdot A_i(t) \quad , \quad i = 1, 2, \ldots \quad . \tag{5}$$

It is worth mentioning, that the decreasing tendency of the total agricultural area has no effect on the regional average of A, due to normalization on the right side. These area mean values of A (specifically the albedo) will be the base of our further calculations.

4. Results

4.1 Surface albedo tendencies

Time series of surface albedo, determined by Eq. (5), represent the result of changes in land use (*Fig. 4*). The surface albedo averaged for the six counties show clear decreasing tendency in the months from April to July (*Fig. 4a*). In other words, the share of those plant species increased, the surface of which is relatively darker in this part of the year (due to, e.g., the larger green mass or more complete cover of the ground). The situation in August is still the same (*Fig. 4b*), whereas no clear change can be established in the two following months. This is in connection with the fact that the majority of the plant species, still present in September–October, can develop longer, so their albedo values become very similar.

As assumed from the total decrease of albedo, regional averages of the surface radiation balance increased in the examined 50 years. Linear trend of

this change is +0.017 W m^{-2} yr^{-1}, which means +0.85 W m^{-2} total change during the examined 1951–2000 period.

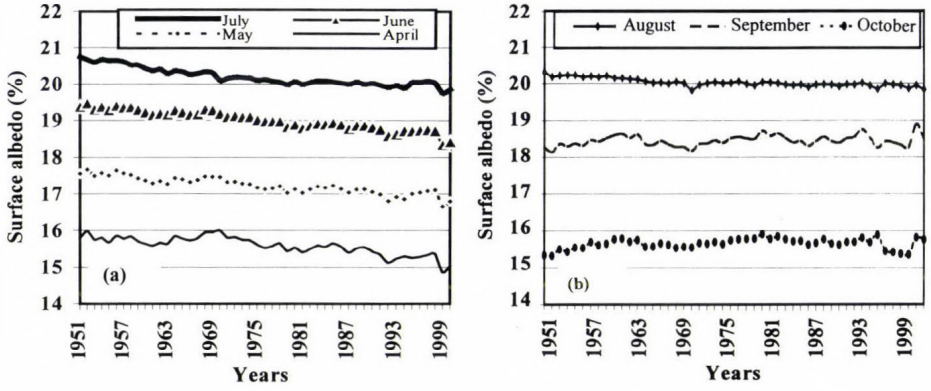

Fig. 4. Effect of land use variations on the surface albedo cumulated for the examined six counties. (a) April–July, (b) August–October.

4.2 Changes in the system albedo

If monthly values of the system albedo are multiplied by astronomically possible solar irradiance, then the amount of shortwave radiation reflected by the surface-atmosphere system to the outer space is received. Changes in this amount can further be compared with other changes in the radiation balance of the system.

The energy surplus, caused by the decreasing radiation energy reflected to the outer space by the surface-atmosphere system, which remains in the system to increase air temperature (longwave radiation), is +0.010 W m^{-2} yr^{-1} (*Fig. 5*), or 0.50 W m^{-2} in total during the examined 50 years. The linear trend fits fairly tightly to the data set, since value of the correlation coefficient is 0.981. (In *Fig. 5*, the changes are demonstrated in comparison to the arbitrarily chosen 1951–1980 period. The point of this operation is not the definite reference period, but the long term basis, instead of any single year with its land use peculiarities.)

Curves of *Fig. 5* also demonstrate considerable county-by-county differences in the slope of the tendency. These changes do not exhibit a clear geographical arrangement. Trends of neighboring counties are quite different in some cases. (The breaks in 1970, recognized in several series, were caused by administrative changes of borders between particular counties. These re-arrangements could not influence the total area or the average albedo of the region.)

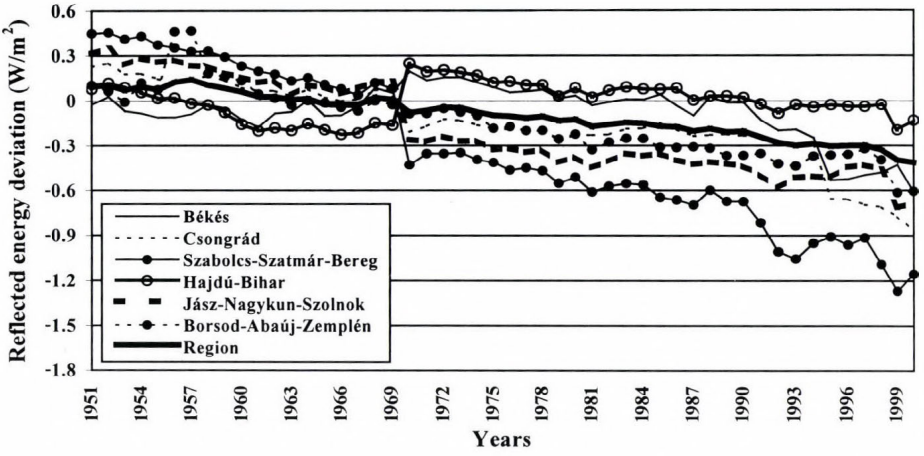

Fig. 5. Effect of land use variations on the reflected energy at the top of the atmosphere for the six counties and the region in April–October, relative to its 1951–1980 averages.

4.3 Comparison to other factors

In order to demonstrate the importance of this relatively small change of the radiation balance, +0.50 W m^{-2}, selected parallel (independent) effects of further forcing factors were computed by the same radiative-convective model (*Table 3*).

Table 3. Estimated direct effect of the documented land-use changes on radiation balance of the surface-atmosphere system compared to selected forcing or feedback mechanisms over Eastern Hungary in the summer half-year.

Forcing or feedback (summer half-year)	**Change (W m^{-2})**
Land use changes 1951–2000	+ 0.50
CO_2 concentration: 330→370 ppm	+ 0.71
Solar irradiance variation: 0.1%	± 0.24
Strong volcanic cloud: $\Delta\tau_{0.55} = 0.1$	- 0.42
Feedback of 0.2 K warming on longwave radiation balance	- 0.54

The effect of CO_2 concentration changes from 330 to 370 ppm (representing the same 1951–2000 period, taken from the corresponding global mean concentrations), is just slightly stronger, +0.71 W m^{-2}.

Result of a hypothetical 0.1% solar radiation variation, which is comparable to the observed fluctuations (*IPCC,* 2001, Chapter 6), is only ± 0.24 W m^{-2}. A strong stratospheric sulfate cloud after a volcanic eruption, characterized by $\Delta\tau = 0.1$ at the 0.55 μm wavelength, can lead to 0.42 W m^{-2} decrease of the radiation balance in Hungary.

On the other hand, this change caused by the land use tendencies is not yet dramatical, since an identical value, -0.54 W m^{-2}, is caused in the longwave part of the spectrum if the near-surface air temperature changes as small as 0.2 K (due to any reason yielding smooth vertical temperature distribution).

5. Discussion

The above mentioned calculations have determined the effect of changes in land use on the albedo and radiation balance. These computations mixed fairly exact *in situ* data on land use with generalized average physical parameters on albedo in combination with a radiation transfer model.

Both components of the calculations request some discussion. The data on land use are based on settlement-level documentation of the corresponding area. Hungary has about 3000 such settlements, so the number of initial data sources used in the area of the present study, i.e., 40% of the country, is well above one thousand. Possible random errors of documentation, therefore, had fairly good chances to be equalized in area mean. For non-random errors one may establish, that except the early periods of the centrally and ideologically planned economy in Hungary, no special interest should be expected on misleading registration of this factor of our computations. Moreover, the basic tendencies of the land use changes, demonstrated in *Fig. 3*, are more general in time.

Another problem with this component might be that the not examined 18–28% of the area (derived from *Table 2*) did not remain constant, either. Area of settlements, transport routes, and water bodies, as well as non-managed (not inventoried) spots of vegetation could also change during the five decades of the analysis. Having no definite data on these processes, however, we can not consider the effects of these changes at present.

As concerns the look-up tables of the applied plants (*Table 1*), two types of error may occur. The first is a possible over- or underestimation of the albedo in average. The other is the possible deviation from this average in the individual years. Both are connected with the way of albedo derivation. The nominal albedo values are based on various projects of direct observations and literature synthesis. They arrange the albedo values according to the

phenological phases. The second step is to identify the average date of the phases within the vegetation period.

The effect of the first source of error is likely not strong. Even if the original 10-day albedo values bear 1–2% absolute error to either direction, they likely decrease during the monthly and further averaging along the vegetation period. On the other hand, the area mean albedo considers almost twenty different types of plant. Likelihood of strong errors, i.e., of the same order of magnitude as the computed effects, is small.

As concerns the errors of albedo estimation in the individual years, they could be larger, especially if the shifts of the pheno-phases, and also the humidity stresses, occurred non-randomly during the fifty years. But, this effect is rather a climate change forced effect, than a land use forced one, since the primary effect of these changes on the albedo of all plants should be more important, than the variations of this primary effect caused by the modified structure of plants coverage within that.

On the above pages, the effects of land use were compared to the components of the radiation balance. According to these comparisons, it could be established that for the region of Eastern Hungary, changes due to land use had the same magnitude as the changes due to the radiation balance occurred in relation with the global climate change or realistic externally forced fluctuations.

It is also worth mentioning, that the continuous decrease of the surface albedo is not only the result of the previous centrally planned economy. The tendencies continued with about the same speed after 1990, too.

However, the question, whether or not changes in land use could produce changes in the regional climate (temperature, precipitation, etc.) with similar magnitude, as the effects of the compared global-scale radiative forcing factors (see in *Table 3*), could not be answered. To answer this question, temporal change of land use should be known for a much larger region, since the climate of Eastern Hungary is influenced by advection of heat and atmospheric water from distant regions. This fact points at shortcomings of the applied radiation-only modeling. This fact, parallel to the obtained significant primary effects on the radiation balance changes, point at the need for sophisticated regional modeling of the land use. Such a regional model should consider all relevant physical processes and a much larger area, even if one focuses on the effects of land use changes just in a part of the whole model domain.

Acknowledgements—The authors are truly indebted to *L. Lukácsovics* for his valuable contribution in series of computations, *Z. Sümeghy* for preparing Fig. 2, *A. Horváth* for her contribution in the data collection, and *I. Kevei-Bárány* for professional advices on integrated classification of the wide variety of vegetation.

References

Central Statistical Office (1951-1993): *Statistical Yearbooks*. Central Statistical Office. County Centres of Hungary

Charney, J.G., Quirk, W.J., Chow, S.H., and *Kornfield, J.*, 1977: A comparative study of the effects of albedo change on drought in semi-arid regions. *J. Atmos. Sci. 34,* 1366-1385.

Claussen, M., 1994: On coupling global biome models with climate models. *Climate Res. 4,* 203-221.

Dávid, A., 1985: Preliminary investigations estimating the regional distribution of surface albedo (in Hungarian). *Beszámolók az 1983-ban végzett tudományos kutatásokról.* Orsz. Meteorológiai Szolgálat, Budapest, 81-98.

de Noblet, N., Prentice, I.C., Joussaume, S., Texier, D., Botta, A., and *Haxeltine, A.*, 1996: Possible role of atmosphere-biosphere interactions in triggering the last glaciation. *Geophys. Res. Lett. 23,* 3191-3194.

Historical Statistical Contributions, (1971-79): *Data on Plant Management* (*Vol. I-IV.:* 1922-33, 34-45, 47-62, 63-70) (in Hungarian). Statisztikai Kiadó, Budapest.

IPCC, 2001: Climate Change 2001: The Scientific Basis. Contribution of Working Group I to the Third Assessment Report of the Intergovernmental panel on Climate Change (Houghton J.T., et al., eds.), Cambridge University. Press, Cambridge, UK. And New York, N.Y. USA, 881 p. http//:www.ipcc.ch.

Karol, I.L. and *Frolkis, A.A.*, 1984: Energy-balance type radiative-convective model of the global climate (in Russian). *Meteorologia i Gidrologia*, No. 8, 59-68.

Liou, K.N., 1980: *An Introduction to Atmospheric Radiation*. Academic Press.

Mika, J., Horváth, Sz., Fogarasi, J., and *Makra, L.*, 1998: Simulation of climate forcing mechanisms on the energy and water balance of a watershed. In *Proc.19th Conf. Danube Countries*, Osijek, Croatia, 15-19, June 1998, 331-342.

Mika, J., Kovács, E., and *Bozó, L.*, 1993: Effects of anthropogenic and natural changes in atmospheric aerosol content on radiation balance in the Carpathian Basin (in Hungarian). *Beszámolók az 1989-ben végzett tudományos kutatásokról.* Orsz. Meteorológiai Szolgálat, Budapest, 81-89.

Mika J., Kovács E., and *Dávid, A.*, 1992: Effect of vegetation and soil conditions on albedo of the surface-atmosphere system (in Hungarian). *Beszámolók az 1988-ben végzett tudományos kutatásokról.* Orsz. Meteorológiai Szolgálat, Budapest, 165-173.

Mika, J., Kovács, E., Németh, P., and *Rimóczi-Paál,* A., 1991: Parameterisation for regional energy balance climate modeling over Hungary. *Adv. Space Res. 11,* (3)101-(3)104.

Mika, J., 1988, Regional features of a global warming in the Carpathian Basin (in Hungarian). *Időjárás 92,* 178-189.

Práger, T. and *Kovács, E.*, 1988: Investigation of effects of atmospheric trace gases and aerosol on climate with a radiative-convective model (in Hungarian). *Időjárás 92,* 153-162.

Rozanov, E.V., Timofeyev, J.M., and *Frolkis, V.A.*, 1981: Effect of trace gases on some characteristics of infrared radiation regime (in Russian). *Izvestii Fiziki Atmosferi i Okeana 4,* 384-391.

Sagan, C., Toon, O.B., and *Pollack, J.B.*, 1979: Anthropogenic albedo changes and the earth's climate. *Science 206,* 1363-68.

Texier, D., de Noblet, N., Harrison, P.S., Haxeltine, A., Jolly, D., Joussaume, S., Laarif, F, Prentice, I.C., and *Tarasov, P.*, 1997: Quantifying the role of biosphere-atmosphere feedbacks in climate change: coupled model simulations for 6000 years BP and comparison with paleodata for northern Eurasia and Africa. *Clim. Dynam. 13,* 865-882.

Warren, S.G., Hahn, C.J., and *London, J.*, 1985: Simultaneous Occurrence of Different Cloud Types. *J. Clim. Appl. Meeorol. 24,* 658-667.

WMO, 1983: *Report of the Experts Meeting on Aerosols and Their Climatic Effects*. Williamsburg, Virginia 28-30 March 1983, World Climate Programme, WCP-55.

Xue, Y. and *Shukla, J.*, 1993: The influence of land surface properties on Sahel climate. Part I., Desertification. *J. Climate 6,* 2232-2244.

IDŐJÁRÁS

Quarterly Journal of the Hungarian Meteorological Service
Vol. 110, No. 1, January–March 2006, pp. 63–87

Application of objective homogenization methods: Inhomogeneities in time series of temperature and precipitation

Péter Domonkos

H-1155 Budapest, Vasvári P. u. 5, Hungary; E-mail: dpeterfree@freemail.hu

(Manuscript received in final form January 12, 2006)

Abstract—Objective homogenization methods (OHOMs) are applied on time series of observed meteorological data mostly from Hungarian sites. The used database comprises temperature and precipitation series at 20 stations from Hungary and 4 stations from other countries in Central Europe. Different ways of data treatment multiply the number of the available series, whereas lack of data limits them. Altogether, 215 series of monthly or annual mean temperatures and 112 series of monthly or annual precipitation totals are analyzed. All of the series are 98–100 years long. The time step between the adjacent members of each series is 1 year. Statistical characteristics of the detected change points, such as mean number of change points per time series, mean magnitude of shifts, etc., are calculated. The aims of the investigation are: (i) to get a general insight into the detectable inhomogeneities in meteorological time series from Hungary, and (ii) to gather the necessary knowledge for the development of testing the efficiency of OHOMs. The study also explains the concept of OHOM, presents its main kinds, and provides some arguments about conditions, advantages, and limitations related to their practical application. Twelve OHOMs are applied in the study, their results have several common features. The OHOMs are taken from the literature with slight modifications, and they are always applied on relative time series, i.e., on the differences of candidate series and reference series. Identical process of reference series derivation, constructed from commonly used elements, is used for all included OHOMs. The main results of the study are: (i) More than half of the examined time series are inhomogeneous. (ii) Most of the detected shift magnitudes are hardly larger than the standard deviation of the noise term. (iii) Serial correlation is indicative of homogeneity quality. (iv) Homogeneity quality of winter temperatures is much better than that of summer temperatures. (v) Distribution of the detected shift magnitudes is skewed positively for each of the OHOMs and each examined meteorological variable.

Key-words: observed time series, homogenization methods, inhomogeneities, temperature, precipitation, Hungary

1. Introduction

The analysis of observed meteorological time series is the main source of our knowledge about climate change and climate variability of the latest centuries. However, reliable consequences about climate variability can be drawn only from databases of high quality. One way of controlling and correcting of observed time series is the use of homogenization methods. These methods check the homogeneous origin of the data, and estimate the necessary corrections for achieving a higher level of homogeneity via comparison of the observed data series in the given region. Thus, the application of a homogenization method supposes a database including several time series of the same meteorological element, these series must have a common time period, and they are supposed to have fairly high spatial correlations (*Peterson et al.*, 1998).

The largest group of the homogenization methods is the group of objective homogenization methods (OHOM). More than 10 kinds of them have been applied in the referred climatological literature so far. During the application of an OHOM on a time series, each decision about acceptance, correction, or rejection of data relies on the statistical characteristics of the time series in the database. Naturally, an application of an OHOM may be supplied with subjectively tailored steps of decision (e.g., with the consideration of contemporary reports, so-called metadata, about the technical or environmental changes in the observations), but all of the OHOMs can be applied without any subjective decisions. Recently, the statistical analysis of large-scale, or even global data sets has become a common tool of detecting climate change and characterizing climate variability. The only way of the quality check in such large data sets is the use of one or more OHOMs. An OHOM recommended for climatological applications must be reproducible, easy-to-use, fast, and suitable for automatic use. Fortunately, most of the OHOMs introduced into the climatology possess these qualities. Thus, the only problem is that which OHOM should be chosen to achieve the highest quality possible of observed data sets? This question will not be answered by the present study, but a large selection of OHOMs is applied together. Results, possibly important for a later development of efficiency testing for OHOMs, will also be discussed.

In this paper we analyze several hundreds of observed time series with the help of twelve OHOMs commonly used in climatology. All of the time series contain monthly or annual mean temperatures or precipitation totals. The length of the series is 98–100 years, and the vast majority of them are originated from Hungarian sites. The organization of the paper is as follows. Section 2 comprises a brief description about the aim, concepts, and tools of

homogenization methods. It is followed by two sections discussing the used database and OHOMs (Sections 3 and 4). Section 5 defines some further methodological details. In Section 6 the calculated statistical characteristics of detected inhomogeneities are presented. The last section comprises discussion and conclusions (Section 7).

2. Theoretical basis

Here we make an attempt to configure the problem of data homogeneity in its most general frame. Some of the formulae and theoretical considerations will be used in the following comparison of OHOMs, too.

A time series from meteorological observations ($\mathbf{X}=[x_1,x_2,...,x_n]^T$) is often expressed as a composition of (a) climatic mean, (b) climatic changes and fluctuations, and (c) errors. Eq. (1) contains more than three components, allowing that both climatic processes and errors may result in long-term changes and short fluctuations in data series. Even an observed climatic mean can be considered as the sum of real climatic mean and the mean of errors. Thus,

$$x_i = \bar{u} + \bar{v} + u'_i + v'_i + u''_i + v''_i \qquad (i = 1,2,...,n), \tag{1}$$

where u and v denote the climatic and local origin, respectively, over line denotes time-average, letters with single comma (u' and v') represent the components of long-term fluctuations, and letters with double commas represent short-term fluctuations approachable usually with white noise. The usual time step between two elements of a time series is 1 year, and it is always 1 year in this study.

All of the components of local origin are error terms, at least from the scope of macroclimatic investigations, but their roles are different during the application of an OHOM. Values of v'' cannot be assessed by statistical tools, since they cannot be distinguished from the short-term climatic fluctuations, unless v''_i is outstandingly high, resulting in an unusual large anomaly of x_i relative to $\bar{x}$. The outstandingly large v'' elements of time series are commonly referred as outliers, and the procedure by which they are recognized and eliminated is the outlier correction. The $\bar{v}$ components can be assessed, but their values are not time dependent. They characterize the spatial representation of individual observing sites and do not affect the homogeneity of the series.

So, the aim of OHOM applications is to identify the $\mathbf{V}'$ vector of time series under examination, and to eliminate its elements from the series. A $\mathbf{V}'$

vector can be considered as the unified term of inhomogeneities of local origin (inhomogeneities, hereafter). If the elements of **V′** are clearly higher than the noise level, and $|v_i| >> |u_i|$ is generally true, the inhomogeneity characteristics can be assessed with fair confidence. By contrast, there is no way of the reliable assessment of inhomogeneities with magnitudes that are lower than the noise level.

If an OHOM is applied on an observed series, the detected inhomogeneities will contain all the long-term changes of the series that are larger than the noise level, either caused by macroclimatic variability or local effects. However, the OHOMs aim to correct the error terms only, and the misidentification or alteration of real macroclimatic terms would be a serious mistake. To distinguish the local effects from the macroclimatic ones, the observed series in question, often referred as candidate series, are usually compared to reference series (**F**) of high quality (considered as homogeneous). Supposing that the macroclimatic effects are the same for the candidate series and the appropriate reference series, their difference, the so-called relative time series (**T**), contains only local effects, already:

$$\mathbf{T} = \mathbf{X} - \mathbf{F}. \tag{2}$$

Although usually no series of an observing network can be considered as absolutely homogeneous, a proper combination of several series from the geographical surroundings of the candidate series is mostly appropriate for the function of reference series. We note that the rate of the **X** and **F** series is also applied as relative time series, for variables whose climatic differences can be characterized better by ratios than by arithmetic differences. However, to keep the theoretical basis in brief, Eq. (2) may also be maintained for the variables of latter type, applying scale transformation on the components of the reference series (see Section 5.1).

As the climatic components cannot be perfectly eliminated by the creation of relative time series (because the **F** series is not perfectly homogeneous, and because of the differences of geographical conditions between the candidate and reference series), **T** contains the same type components as **X** in Eq. (1). Notwithstanding, the relative importance of the individual components is changed. Using a proper reference series, the absolute values of u' elements are practically never higher than the noise level. Thus, unifying the mean terms to $\bar{t}$ and the noise terms to e, Eq. (1) can be rewritten for relative time series in the form of

$$t_i = \bar{t} + v'_i + e_i. \tag{3}$$

If a time series is homogeneous, then every elements of $\mathbf{V}'$ are equal to 0. As the reference series are supposed to be homogeneous, the inhomogeneities of a relative time series are attributed to the candidate series. In this study, OHOMs are applied always on relative time series.

The most common type of inhomogeneities is the so-called change point. A station movement, an abrupt methodological change in the observation timing or instrumentation, or some changes in the neighborhood of the station usually cause sudden shift in the average values of the observed data. If $\left|v'_j - v'_{j-1}\right| >> 0$ $(1 < j \leq n)$, it indicates a change point at year j. While the appearance of an existing change point may be obscured by the noise around year j, on the other hand, unusual structure of noise may have an appearance similar to change points. Therefore, the success of change point identification has a stochastic character, and it strongly depends on the rate of abrupt change to the noise level (*Ducré-Robitaille et al.*, 2003). Another typical form of inhomogeneities is a long-lasting, trend-like change in the values of the time series. They are caused by the gradual changes of some instrument characteristics or, more frequently, by the gradual changes in the site environment, e.g., in connection with the growing urbanization. The appearance of this type of inhomogeneities in the terms of Eq. (3) is a gradual, monotonous change in the v' components.

Further explanations of concepts of homogenization are delivered by *Alexandersson* and *Moberg* (1997), *Peterson et al.* (1998), *Sneyers* (1999), and others.

3. Database

Six different databases of monthly mean temperatures or monthly precipitation totals were chosen to assess the characteristics of detectable inhomogeneities. The meaning of "six different databases" is as follows: Any pairs of data series belong to the same database if they contain the data of the same meteorological variable (temperature or precipitation), and if they are likely derived by the same preprocessing, as considered from the documentation that accompany the series. None of the databases used here were subjected to an OHOM before our analysis.

Most of the data series are delivered by the Hungarian Meteorological Service, and more than 90% of the series comprise observed data from Hungarian sites. (The few exceptions are temperature series from Prague, Cracow, Zagreb, and Bologna; see *Table 1*.) All of the six databases had been used earlier in climatological works, thus we consider all of them equally relevant. For an easier wording, different initial databases are referred as

"different sources" hereafter, and the word "database" is held for the whole set of data series.

Table 1. Data series of observing sites, included in the individual data bases. (I,...,IV mark the distinction according to previous data treatment; T and P denote temperature and precipitation, respectively.)

Stations	**Longitude**	**Latitude**	**I**		**II**		**III**	**IV**
	(E)	**(N)**	**T**	**P**	**T**	**P**	**T**	**T**
Bologna, IT	11°20′	44°30′						+
Prague, CZ	14°25′	50°05′						+
Zagreb, HR	15°59′	45°49′						+
Cracow, PO	19°58′	50°04′						+
Sopron	16°36′	47°41′			+	+	+	
Szombathely	16°36′	47°15′	+	+	+	+	+	
Zalaegerszeg	16°49′	46°55′	+	+				
Keszthely	17°14′	46°44′			+	+		
Mosonmagyaróvár	17°16′	47°53′	+	+	+	+	+	+
Pápa	17°22′	47°18′	+	+				
Győr	17°41′	47°43′		+				
Kaposvár	17°50′	46°22′	+	+				
Iregszemcse	18°11′	46°41′	+	+				
Pécs	18°14′	46°00′	+	+	+	+	+	
Budapest	19°02′	47°31′	+	+	+	+	+	
Baja	19°11′	46°11′			+	+		
Kecskemét	19°46′	46°54′	+	+	+	+	+	
Szeged	20°09′	46°15′	+	+	+	+	+	+
Szarvas	20°33′	46°52′			+	+		
Túrkeve	20°45′	47°06′			+	+		
Miskolc	20°46′	48°07′	+	+			+	
Békéscsaba	21°06′	46°41′		+				
Debrecen	21°37′	47°33′	+	+	+	+	+	+
Nyíregyháza	21°41′	47°59′	+	+	+	+	+	
All elaborated			**13**	**15**	**13**	**13**	**10**	**7**

The data series are complete, their length is 98–100 years, and all of them cover the period 1901–1998. The time step between two adjacent elements of the series is always 1 year. We use the series of values from central months of

traditional seasons (January, April, July, and October), as well as series of annual values. The month (or the whole year), to which a series belongs, is referred as seasonality of the series, throughout the paper. A group of data series, whose source and seasonality are common, is labeled data segment. There is no difference in the length of the series within a segment. Considering that there are 6 initial databases (see *Table 1*) and 5 types of seasonality (central months of the four seasons as well as the entire year), the possible maximum number of elaborated data segments would be 30. However, the final number of segments really used is 28, because two possible segments comprising precipitation in July are omitted, due to too low spatial correlations (see Section 5.1). Each segment consists of 7–15 time series (with an average number of 11.8), thus the whole database comprises 327 time series, i.e., 215 temperature series and 112 precipitation series.

4. Homogenization methods applied

Twelve OHOMs are applied in this study. As general rules, all the OHOMs were used in broadly available climatological studies earlier, their theoretical bases and practical application are published in scientific journals, and they are reproducible from these papers and other available guides or descriptions. Nevertheless, there are some exceptions to these rules, they will be discussed together with a more extensive description of the individual OHOMs applied in this study.

The twelve OHOMs and their abbreviations are as follows:

(i) Buishand-test of the maximum accumulated anomaly [Bs1],
(ii) Buishand-test of the difference between the maximum and minimum of accumulated anomalies [Bs2],
(iii) Wilcoxon Rank Sum statistic [WRS],
(iv) Pettitt-test [Pet],
(v) Mann-Kendall test [M-K],
(vi) Standard Normal Homogeneity Test for shifts only [SNH],
(vii) Standard Normal Homogeneity Test for shifts and trends [SNT],
(viii) Multiple Linear Regression [MLR],
(ix) Bayesian approach [Bay],
(x) method of Easterling and Peterson [Eas],
(xi) a version of the Multiple Analysis of Series for Homogenization [MS1],
(xii) another version of the Multiple Analysis of Series for Homogenization [MSH].

Ten methods from the twelve OHOMs look only for change points, whereas two of them (SNT and MLR) can recognize shifts and trends alike.

Usually, the identification of change point positions in time is the critical point of the effectiveness of an OHOM, although, the assessment of its statistical significance and the measure of the jump (i.e., the shift-magnitude) are also very important.

Now, let us describe the above listed 12 OHOMs. Perhaps the oldest homogenization method is the investigation of the accumulated anomalies (*Kohler*, 1949). A sudden shift in the values of the examined series tends to cause a local maximum or minimum in the accumulated anomalies. Bs1 and Bs2 (*Buishand*, 1982) are OHOMs relying on the analysis of accumulated anomalies.

The frequencies of positive and negative relations between sample elements chosen from the different sides of a change point are biased from equality (50–50%), and the measure of the bias has a local maximum around the change point. This is the basic idea of OHOMs calculating frequencies of relations between sample elements or constructing statistics for rank-ordered sample. WRS (*Karl* and *Williams*, 1987), Pet (*Pettitt*, 1979), and M-K belong to this group. We applied the M-K test relying on the description by *Aesawy* and *Hasanean* (1998), but with the supplement of serial correlation analysis. The calculation of serial correlation is a traditional way of indicating homogeneity or inhomogeneity of a time series. About serial correlation analysis see, e.g., *Sneyers* (1997, 1999). The supplement to the M-K test is needed, because otherwise this test tends to find too many change points, even in a pure white noise process.

The Standard Normal Homogeneity Test (often referred as SNHT) is the OHOM which has most frequently been applied by climatologists in the recent years. It relies on the fact that differences in the means of any two adjacent sub-periods, covering together the whole series, have a local maximum at a change point. Two versions of this approach are applied. While the SNH version (*Alexandersson*, 1986) assesses and corrects only the change point type inhomogeneities, SNT is able to recognize gradual changes, too (*Alexandersson* and *Moberg*, 1997). Gradual changes recognized by SNT are modeled with linear changes in certain sections of the series.

Another group of OHOMs applies fitting of predefined function types, such as constant sections with shifts between them, linear changes, etc. The optimal function is the one with minimum root mean square error (RMSE). MLR (*Vincent*, 1998) represents this type. It is capable of recognizing and correcting both abrupt shifts (change points) and gradual changes. The original Bayesian approach (*Ducré-Robitaille et al.*, 2003) also belongs to this group. However, in this study a part of that method is applied, namely the derivation of the most probable change point position. In the Bay method applied here, the Bayesian derivation of change point position is supplied with serial

correlation analysis for controlling significance, and the way of the assessment of shift magnitudes is an unchanged adaptation from the SNH test.

The method Eas developed by *Easterling* and *Peterson* (1995) is a multi-step procedure. It starts with the fitting of one or two straight lines with the minimum RMSE. If the fitting of two lines (with a sudden shift and/or a break in the trend line) is significantly better than the fitting of one line, a potential change point is flagged to the position of the break, and the series is cut into two sub-periods at this point. This step is repeated for the sub-periods as long as one line has a better fitting than any two lines. Thereafter, the significance of the flagged inhomogeneities is controlled one-by-one, applying rank order statistic in windows with maximum 12 years half-windows towards either side from the flagged inhomogeneity.

The Multiple Analysis of Series for Homogenization (often referred as MASH) is a development of a Hungarian mathematician. The full description of the method is available in a WMO conference issue (*Szentimrey*, 1999), with abbreviated information in the review paper by *Peterson et al.* (1998). MASH is a rather complex method, its application needs much more computing time, than that of the other OHOMs. The MASH method examines all the possible change point configurations in a time series using dynamic window width. Examining a sub-period with a given window, the flagging of potential change points is based on special statistical criterion, similar to the one in SNH. The optimal set of change points is determined by a multi-step iteration procedure. MSH is the developer's original software. MS1 contains some modifications. The main difference between the two versions is that the minimum width of the half-windows is 5 years in the MS1 method (1 year in the original version).

Moberg and *Alexandersson* (1997) give instructions how to identify multiple inhomogeneities. Their advice is for the use of SNH and SNT, in fact, but it is also applicable and beneficial for many other OHOMs. These instructions are as follows. (a) If a change point is found, the position of this pre-detection is flagged, and the time series is cut into two sub-periods at the time point of the pre-detection. If a gradual change is found, its endpoints are flagged, and the first sub-period lasts until the first flag, and the second sub-period begins from the second flag. (b) Sub-periods not shorter than 10 years are examined for further inhomogeneities. (c) The first phase of the examination is finished when no further inhomogeneity is detectable in the sub-periods. (d) The second phase of the detection procedure begins. Its name is backward testing of inhomogeneities. Pre-detected inhomogeneities are checked one-by-one, starting from the end of the time series. In an individual step, a sub-period with only one inhomogeneity (flagged in the first phase) is examined, and the correction, assessed from the ongoing step, is applied

promptly. Therefore, the applied window in the backward testing of a pre-detected inhomogeneity stretches from the time point of the left hand side adjacent inhomogeneity pre-detected to the end of the series. (There are no inhomogeneities to consider on the right hand side of the series in this phase, because they have already been corrected.)

During the applications of OHOMs, we follow the above instructions with some slight modifications. (a) Not only the minimum length of any sub-periods for further examinations is given, but the minimum size of the half-windows is fixed as 5 years. (b) The corrections are not applied promptly after the individual steps of the second phase, but their influence is eliminated applying shorter windows, so that time windows stretch only to the adjacent inhomogeneity on the right hand side of the time series.

The rules above are applied in most of the OHOMs, but the Eas, MS1, and MSH methods are exceptions, since they have own solution to how to treat the multiple inhomogeneities. In the MS1 method the maximum half-window length is 5 years, so this parameter of MS1 is set to be identical with those of the other OHOMs.

5. Derivation of relative time series

We intend to apply the homogenization procedures described in the previous section on all of the 327 time series specified in Section 3. Before application, however, relative time series are created for each observed series, referred also as parent series hereafter, and all of the homogenization procedures are performed on these relative time series.

The creation of relative time series needs the determination of a reference series for each parent series (see also Section 2). Another task is to convert relative time series into a standardized mode, for which the statistical characteristics of inhomogeneities, detected in relative time series, are comparable, despite the fact that the basic statistical properties of parent series are very different. Therefore, this section is divided into two parts: in the first part the building of reference series is presented, then the standardization method of relative time series is described.

5.1 Building of reference series

We follow the method proposed by *Alexandersson* and *Moberg* (1997), but with certain modifications. Before starting, the series of precipitation data are subjected to scale transformation to eliminate differences in ratios. Temperature is basically an additive variable, so ratio differences are not considered for that.

In Eq. (4) x denotes raw precipitation data, and x^* denotes transferred data. The scaling factor is the reciprocal rate of the time average for the series under transformation, relative to the spatial-temporal average for the whole data segment.

$$x^*_{j,i} = \frac{\frac{1}{M}\sum_{m=1}^{M}\overline{X_m}}{\overline{X_j}} x_{j,i} \qquad j \in (1,2,...M), \tag{4}$$

where M is the number of data series within a data segment, j denotes the time series that is just under transformation, and

$$\overline{X} = \frac{1}{n}\sum_{i=1}^{n} x_i \,. \tag{4a}$$

After fulfilling this transformation, Eq. (2) is applicable both for temperature and precipitation time series. We mention that *Alexandersson* and *Moberg* (1997) propose a transformation of making 0 time average for all time series (uses anomalies from $\overline{X_m}$). However, this step may be omitted, because all the time series in any of the data segments (built in Section 3) cover exactly the same period.

The values of reference series are determined by Eq. (5). According to it, the reference series **F** originates from K data series of the data segment including the candidate series. All of the series have the same, n years length.

$$f_i = \frac{\sum_{m=1}^{K} r_m^2 x_{m,i}}{\sum_{m=1}^{K} r_m^2} \qquad i = 1,2,...,n. \tag{5}$$

The factor r_m^2 depends on the spatial correlation between the candidate series and the time series marked by m. More precisely, r_m is the spatial correlation for the series of differences (**D**) between the adjacent elements of data vectors, between the candidate and the $\mathbf{X}_m$ series. The calculation of the elements of **D** is shown in Eq. (6).

$$d_{m,i} = x_{m,i} - x_{m,i-1} \qquad i = 2,3,...,n. \tag{6}$$

Data series with relatively high r values may compose a reference series, because low spatial correlation indicates substantial geographical difference, which likely contains climatic differences, too. The use of difference series instead of the original **X** series in the calculation of spatial correlations has a

considerable advantage, namely, the correlations are less affected by inhomogeneities, thus they indicate geographical coherence with higher reliability.

Alexandersson and *Moberg* (1997) do not give concrete instructions how to chose the K number of the utilized data series in the building of reference series. It is not an easy task to set general rules for this, which would operate well in a wide range of conditions, because the optimal selection of the series depends on several factors. For example, a utilized data series must be representative spatially, must have a rather high correlation with the candidate series, must have a fairly high quality, etc. It is favorable, if there are composites of the reference series from all of the four main geographical directions, but this rule would be applicable only on large data segments of dense observing networks.

We introduce some simple criterions for selecting data series composing reference series. Using these criteria, the automatic building of reference series, related to a given candidate series, is possible in the following steps. (1) The time series, which are potentially useful for spatial comparison, i.e., the other series of the data segment of the candidate series, are ordered according to the spatial correlation with the candidate series (r), and series of the highest r values are selected. (2) The threshold r_t above which time series are included in the reference building is not a constant, but it depends on the number of series selected in the previous steps. If there is a large number of series with high spatial correlations, a relatively high r_t threshold can be chosen, and vice versa. (3) The threshold r is not allowed to be lower than 0.7. (4) The minimum number of selected composites is 2, otherwise reference series cannot be built to the candidate series, and the homogeneity test is rejected.

A proper formula was constructed to satisfy all the above criteria. The change of r_t in the function of the serial number (m) of the series under examination is given by Eq. (7). The first four values are constant (0.7), then r_t rises with m exponentially, faster at first, slower later, and it approaches asymptotically to 1 (*Fig. 1*).

$$\begin{aligned} r_{t,m} &= 0.7 && (1 \le m < 4), \\ r_{t,m} &= \sqrt{1 - p(1 - r_{t,m-1}^2)} && (5 \le m < M), \end{aligned} \tag{7}$$

where p was chosen to meet the arbitrary condition of $r_{t,5}=0.72$, thus $p=0.9443$.

The spatial correlations between temperature values are well above 0.7 within the small area covered by the Hungarian observing network. Even in the particular data segment supplemented by temperature series from a larger

area (i.e., from Bologna to Cracow), the spatial correlations are still sufficient to build reference series. (The only exception is Bologna, for July, for which the second largest spatial correlation is only 0.688, also accepted by a specific decision to build the reference.)

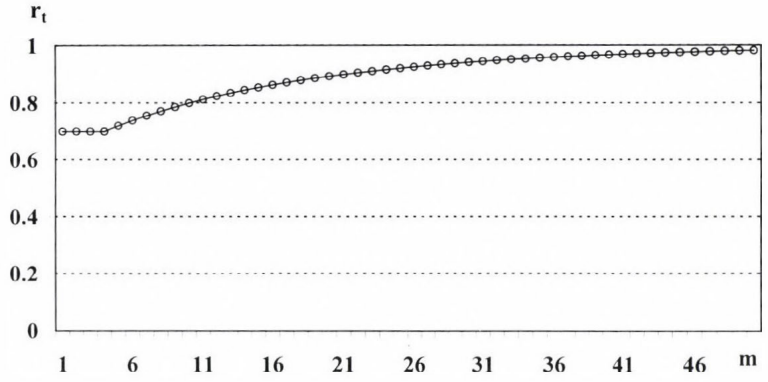

Fig. 1. Minimum threshold of spatial correlation (r_t) for the inclusion of time series into the process of building reference series. *m* means the *m*th highest spatial correlation between the candidate series and any other series of the data segment.

However, the correlation between precipitation series declines with distance much faster, than in case of temperatures. Correlation coefficients between precipitation series are particularly low in late spring and in summer, when considerable part of precipitation is of convective origin with rather hectic spatial distribution. Therefore, segments comprising July precipitation totals were excluded from the whole investigation. The correlation coefficients for April are substantially higher than those for July, thus all the series of April precipitation are included, although with some compromise in r_t values. Namely, r values between 0.64 and 0.7 were accepted if there was no other possibility to build the reference series. There were no problem in building of reference series for January, October, and annual precipitation totals.

5.2 Standardization of relative time series

When the results of an OHOM is under evaluation, the typical size of the detected shifts is a major characteristic to consider. However, how could one compare a 1 °C shift in temperature with a 20 mm shift in precipitation? Even the importance of a 1 °C shift is likely different for time series of monthly

values, than for annual values. These examples show that standardization is needed before the comparison of detected inhomogeneities. Naturally, this standardization can already be performed before the homogenization procedure. The way, how we fulfilled this task is specified in the following.

It seems to be simple to express the inhomogeneity magnitudes in proportion to the empirical standard deviation of the time series (s_T). However, s_T itself also depends on inhomogeneities in the series. If these inhomogeneities are relatively large, then the standard deviation is considerably larger, than that for the homogeneous series. This feature of s_T would cause undesired biases in the results.

Theoretically, the standard deviation of the white noise component (s_e) would be the optimal reference unit to which the inhomogeneity magnitudes can be related, but this component is not known exactly. Nevertheless, the following estimate of the unit is closer to s_e than the empirical standard deviation of the series. The core of the concept is to reduce s_T with the variability related to the serial correlation (r_s), since that part of the variability is obviously not white noise:

$$s_e^* = \sqrt{1 - r_s^2}\, s_T \,. \tag{8}$$

For Markovian processes, Eq. (8) provides an exact determination of the standard deviation of the noise, thus for those processes $s_e = s_e^*$. Although in real climatic time series s_e^* is always larger than the pure white noise, s_e^* is considered to be the standard deviation of the noise process in the study, and that is the reference unit of the detected inhomogeneities, if there is no indication of using another unit.

6. Results

Statistical characteristics of the detected inhomogeneities are presented here. Change point type inhomogeneities are under study at present.

The section consists of three parts. First, the inhomogeneity characteristics of the annual mean temperature series are shown, and results from the different OHOMs are compared. Second, inhomogeneity characteristics of other meteorological variables are compared with those derived for the annual mean temperature series. In the third part, the investigated time series are classified in another way, i.e., according to the similarity of their serial correlations, not considering the type of the meteorological variable they characterize.

6.1 Inhomogeneities in the series of annual mean temperatures

Annual mean temperature series are more frequently subjected to homogenization investigations than any other type of meteorological time series. The possible reasons are as follows. First, air temperature is a fundamental environmental variable. Thus, it is important to reveal its trends and low frequency changes relatively precisely. Second, its instrumental observation usually goes back to several decades or centuries. Third, the homogeneity of temperature series is very sensitive to technical conditions, hence, it is often affected by methodological or environmental changes. Fourth, networks for temperature observations generally have adequate density for ensuring sufficient spatial correlations, thus relative time series with fairly low noise level can be created. Homogeneity of annual mean temperature series has recently been examined, e.g., by *Jones* and *Lister* (2004) for Scotland and Northern Ireland, by *Türkes et al.* (2002) for Turkey, by *Alexandrov et al.* (2004) for Bulgaria, by *Domonkos* and *Tar* (2003) for Hungary, and by *Wijngaard et al.* (2003) for the whole data base of the European Climate Assessment project. We note that the examination of seasonal mean temperatures is in focus in several other studies (e.g., *Kyselý*, 2002; *Tomozeiu et al.*, 2002).

Table 2. Statistical characteristics of detected inhomogeneities in series of annual mean temperatures from observations: (a) rate of series found to be inhomogeneous, in %, (b) mean number of detected change points for inhomogeneous series, (c–e) moments of the shift magnitudes: (c) average, (d) standard deviation, (e) skewness

	a	b	c	d	e		a	b	c	d	e
Bs1	91	2.6	1.6	0.8	2.1	SNT	84	1.7	1.8	1.0	1.9
Bs2	95	2.9	1.6	0.8	1.9	MLR	100	2.6	1.8	0.9	1.6
WRS	86	2.1	1.6	0.8	3.2	Bay	100	3.3	1.7	0.9	1.6
Pet	91	2.7	1.5	0.8	2.6	Eas	91	2.0	1.9	0.9	2.4
M-K	100	2.3	1.3	0.8	1.3	MS1	98	3.1	1.8	0.9	1.6
SNH	84	2.5	1.7	0.9	2.1	MSH	98	3.2	1.9	0.9	1.6

In our investigations, 43 relative time series, derived from series of annual mean temperatures in four data segments, are examined with the twelve OHOMs listed in Section 3. *Table 2* shows the basic statistical properties of the detected inhomogeneities. The application of OHOMs indicates significant inhomogeneities in almost all series. More precisely, only 0–7 series are found

to be homogeneous (depending on the type of the OHOM), and 36–43 series were inhomogeneous from the investigated 43 series. Usually, multiple change points are detected, the average number of change points in an inhomogeneous series is between 1.7 and 3.3. However, the mean shift magnitude is low, it is always below 2. (Note, that this is a relative number, representing the proportion of the inhomogeneity shift to the noise term s_e* introduced in Section 5.2) The standard deviation of shift magnitudes is large in comparison with their average values. There are no great differences in the averages and standard deviations, calculated by the different methods.

The skewness values show slightly larger dependence on the applied method, but all of them are positive, and none of them is lower than 1. It means that most of the detected shifts are small, i.e., smaller than the average values, shown in columns "c" of *Table 2*.

The distribution of the detected shift magnitudes is illustrated in *Fig. 2*. The three curves of the figure represent the averaged results of 4-4 OHOMs. Curve (A) is for the OHOMs yielded relatively low magnitudes, curve (B) is for the OHOMs resulted in relatively few change points, and curve (C) is for the OHOMs indicating large number of change points often with relatively high magnitudes.

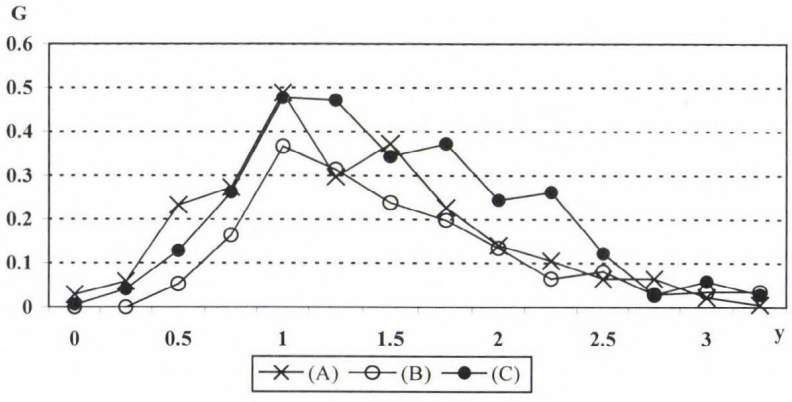

Fig. 2. Distribution of the detected shift magnitudes (*y*) in the series of annual mean temperatures. *G* indicates the mean number of occurrence per time series for predefined sections of the *y* values. Each curve is an average for four OHOMs. (A) Bs1, Bs2, Pet, M-K; (B) WRS, SNH, SNT, Eas; (C) MLR, Bay, MS1, MSH.

Although the three curves in *Fig. 2* and the content of *Table 2* demonstrate systematic differences between the individual OHOMs, these

differences are not very large, and some general features of the results are approximately uniform. The most important common features are (i) the indication of the change points in almost all of the series, and (ii) the predominantly low shift magnitudes. It is worth mentioning, that in case of an ideal equal distribution of shift magnitudes, the distribution of the detected magnitudes by OHOMs would show negative skewness, because the proportion of successful detection is higher for the large shifts than for the small ones *(Ducré-Robitaille et al.*, 2003). It suggests, that the positive skewness of the distribution of real shift magnitudes is even larger than that shown in *Fig. 2*.

6.2 Comparison of detected inhomogeneities for different meteorological variables

Data segments are sorted into five groups according to the type of meteorological variables: (i) annual mean temperature, (ii) July temperature, (iii) monthly mean temperature in transition seasons (April and October), (iv) January temperature, (v) monthly or annual precipitation total. The number of data series in the classes (i)–(v) is 43, 43, 86, 43, and 112, respectively. The class of precipitation total is not divided into smaller groups according to seasonality, because the frequency of detected change points is too low for a separate examination of monthly precipitation totals.

Four OHOMs are chosen for the comparative examination. They are Bs2, WRS, SNH, and MS1. All these OHOMs focus on detecting the change points, and their efficiency seems to be fairly good according to a preliminary study (*Domonkos*, 2005). *Fig. 3* shows the distribution of shift magnitudes for each class of meteorological variables. The shape of the curves is rather similar, albeit the frequencies of the detected change points are clearly different. The most change points are detected in the annual temperature series, followed by the July temperature series. Relatively few change points are detected in the precipitation series. There is a robust difference between the frequencies of detected change points in the different seasons. Inhomogeneities are much more frequent in summer than in winter: while 77–86% (depending on the applied OHOM) of the temperature series are found to be inhomogeneous in July, this rate is only 12–35% for the January temperatures.

In spite of the large differences among the total frequencies, the most frequent shift magnitude is almost the same for the examined classes of series. Shifts, whose magnitudes are close to the assessed noise level, are detected most frequently, whereas magnitudes above 2 (or above 2.5 for the annual temperatures) are very seldom, compared to the frequencies of smaller inhomogeneities.

Although inhomogeneity magnitudes are usually expressed in the proportion of the noise standard deviation (s_e*), the content of *Fig. 3* is presented also in physical units, i.e., °C for temperatures (*Fig. 4*) and mm for precipitation totals (*Fig. 5*). Beyond the differences of the applied units, another difference between *Fig. 5* and the class (v) of *Fig. 3* is that only annual totals were considered in the calculations for *Fig. 5*.

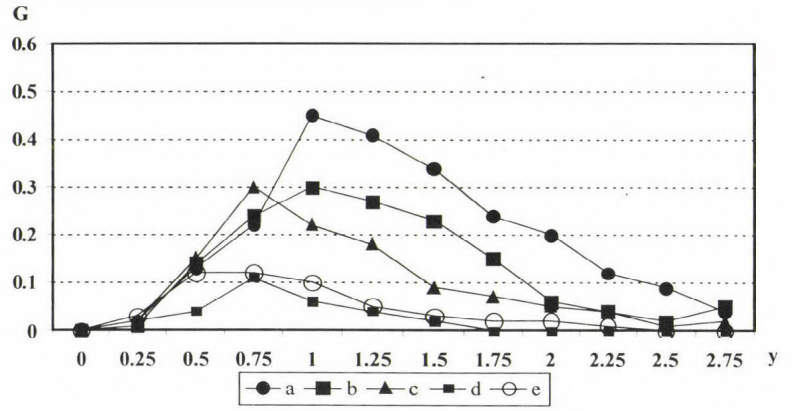

Fig. 3. Distribution of the detected shift magnitudes in the proportion of assessed standard deviation of noise. (a) annual mean temperature, (b) July mean temperature, (c) monthly mean temperature for April or October, (d) January mean temperature, (e) monthly or annual precipitation total.

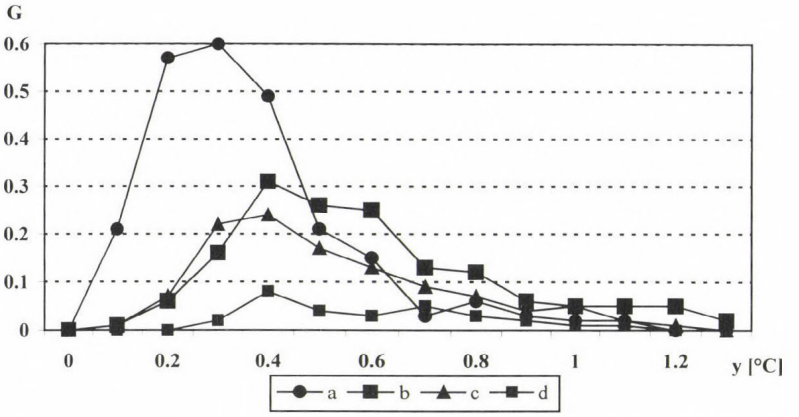

Fig. 4. Distribution of the detected shift magnitudes in temperature series, expressed in °C. (a) annual mean temperature, (b) July mean temperature, (c) monthly mean temperature for April or October, (d) January mean temperature.

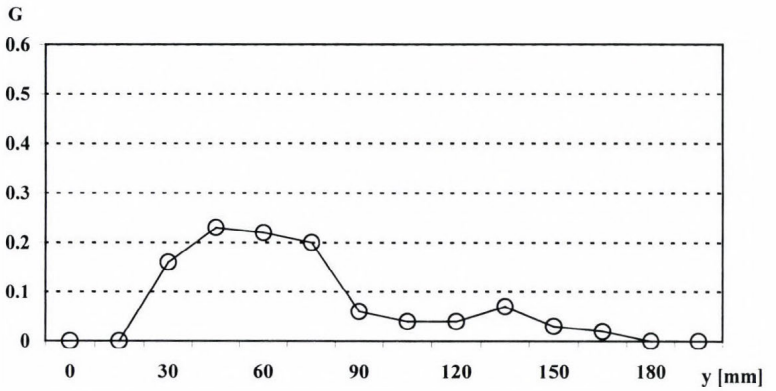

Fig. 5. Distribution of the detected shift magnitudes in time series of annual precipitation totals expressed in mm.

Fig. 4 confirms the main point of *Fig. 3*: the vast majority of the detected inhomogeneities is small. While the most large or medium shift magnitudes were found in the annual mean temperatures in *Fig. 3*, series of July temperatures have the most, relatively large inhomogeneities in the absolute scale. The annual mean temperature series have outstandingly large number of shifts in the range of 0.2–0.5 °C. For the monthly temperatures, the peaks of the magnitude distributions are flatter, and their typical range is 0.3–0.7 °C. Occurrence of shift magnitudes around or above 1 °C is much less frequent than that of the small shifts.

In the series of annual precipitation totals, fewer change points are detected than in the most temperature series, but these magnitudes are not very small. A flat peak of frequency appears between 30 mm and 90 mm, and these values are in the order of 1/10 of the climatic average for annual precipitation totals. While smaller than 30 mm shift magnitude has not been detected at all, the right hand tail of the distribution is long, with occurrences of 100–180 mm magnitudes. On the other hand, 20–50 percent (depending on the applied OHOM) of the annual precipitation series was found to be homogeneous.

All of the magnitude distributions, examined so far, have positive skewness. It strengthens the finding of Section 6.1, that the rate of small inhomogeneities is very high among the existing inhomogeneities. Theoretically, the experienced magnitude distributions of detected inhomogeneities may be composed in two possible ways: (a) There are numerous series with only small inhomogeneities, but a few series contain one or more large shifts instead of small inhomogeneities; (b) Small inhomogeneities are commonly present in time series. If a large shift occurs, its identification is relatively

difficult due to detectable or hidden small inhomogeneities. In the last part of this section, the relative time series are grouped in another way. The examination of groups independent from the parent data segments will give the answer to this question.

6.3 Classification of data series according to serial correlation

Serial correlation indicates the homogeneous or inhomogeneous character of a time series (see Section 4). Thus, the properties of detected inhomogeneities for classes of specified serial correlation ranges may be informative. *Table 3* shows the numbers of data series under study, for certain classes of serial correlation, r_s. Considering that $r_s > 0.25$ values are significant on the 0.01 level for a 100 years long time series, 40% of the series have substantially positive serial correlation. A small fraction (7.6%) of the series shows definitely high, at least 0.6 serial correlation.

Table 3. Numbers of data series in certain classes of serial correlation (r_s)

Class	r_s	Number of data series
Ra	< 0.15	137
Rb	0.15–0.25	59
Rc	0.25–0.40	59
Rd	0.40–0.60	47
Re	0.60 ≤	25

Fig. 6 shows the distribution of detected shift magnitudes for r_s classes in the same way, as *Fig. 3* does for specified meteorological variables. Also, the four OHOMs applied are the same in these figures. *Fig. 6* illustrates that higher serial correlation coefficients generally indicate more frequent and larger shifts in a time series, than lower r_s values. However, the highest frequency of shift magnitudes appears close to the noise level for each class, and frequency of around or above 2.5 is definitely rare, even for the class of uppermost serial correlations. It seems that the dominance of small shifts is very general, and series with merely large shifts are very seldom.

Table 4 presents further details about inhomogeneity properties for certain classes of serial correlation. It can be seen that serial correlation values above 0.25 are indicative of inhomogeneity, indeed. Examining the occurrence frequencies and mean magnitudes of the shifts, one may find substantial dependence on OHOMs, but the differences between the characteristics for

classes of the lowest and highest serial correlation coefficients are usually larger than the method dependence. Skewness values are always positive, again, and they are particularly high for the class of high serial correlation.

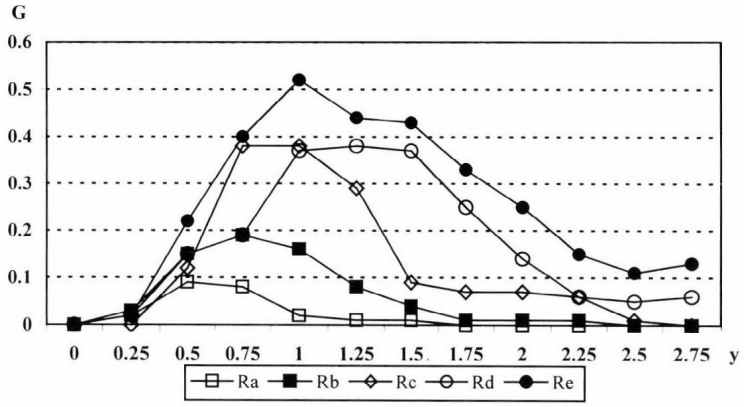

Fig. 6. Distribution of detected shift magnitudes for classes of serial correlation (r_s). Ra: $r_s < 0.15$, Rb: $0.15 \le r_s < 0.25$, Rc: $0.25 \le r_s < 0.4$, Rd: $0.4 \le r_s < 0.6$, Re: $r_s \ge 0.6$.

Table 4. Statistical characteristics of inhomogeneities for time series in certain classes of serial correlation

Serial correlation	Bs1	Bs2	WRS	Pet	M–K	SNH	SNT	MLR	Bay	Eas	MS1	MSH
	Rate of inhomogeneous series (%)											
< 0.25	28	26	24	31	25	25	26	27	27	34	42	43
0.25–0.4	81	86	80	88	95	81	81	98	98	71	100	98
≥ 0.4	96	100	96	96	100	94	94	100	100	93	100	100
	Mean number of change points in inhomogeneous series											
< 0.25	1.2	1.1	1.1	1.3	1.1	1.3	1.1	1.1	1.3	1.1	1.4	2.1
0.25–0.4	1.6	1.6	1.4	1.7	1.7	1.5	1.2	1.9	2.2	1.5	2.1	2.3
≥ 0.4	2.5	2.7	2.1	2.5	2.3	2.4	1.7	2.6	3.3	1.9	3.1	3.3
	Mean magnitude of shifts											
< 0.25	0.8	0.8	0.9	0.8	0.7	1.0	1.0	1.0	1.0	1.2	0.9	1.6
0.25–0.4	1.1	1.2	1.2	1.1	0.8	1.3	1.3	1.3	1.3	1.4	1.4	1.5
≥ 0.4	1.6	1.6	1.6	1.5	1.3	1.7	1.8	1.8	1.7	1.8	1.7	1.8
	Skewness of shift magnitude distribution											
< 0.25	0.9	0.4	1.7	0.7	0.2	1.1	1.1	0.8	1.0	1.2	1.1	1.0
0.25–0.4	1.2	1.7	1.1	1.2	0.6	1.3	1.5	0.7	0.4	0.8	0.8	0.9
≥ 0.4	2.5	2.1	3.1	2.5	1.1	2.2	1.8	1.8	1.7	2.4	1.9	1.7

7. Discussion and conclusions

Homogeneity characteristics of 327 time series, mostly Hungarian temperature and precipitation series, were investigated applying twelve objective homogenization methods (OHOMs). It was found that at least half of the series in the data base (50–65%, depending on the OHOM applied) contain significant inhomogeneities. However, most of the detected inhomogneities are small, their magnitudes are scattered around the noise level. A small part of the inhomogeneities are 2–3 or even more times larger than the noise level.

The highest frequency of inhomogeneities was found in the series of annual mean temperatures, followed by the series of July temperatures. Relatively few inhomogeneities were found in the series of precipitation totals, and very few in the series of January temperatures. Nevertheless, the relatively lower frequency of the detected inhomogeneities in precipitation series does not prove high quality for those demonstrated by the rather high absolute magnitudes of shifts in the time series of annual precipitation totals (*Fig. 5*). The explanation is the relatively low spatial correlations among precipitation time series, which result in higher noise levels of relative time series from precipitation totals, in comparison with series from mean temperatures.

The results for January temperatures need different explanation. In this case the spatial correlation coefficients are very high, but the frequency of the detected inhomogeneities is the lowest. These results together indicate a really high quality of the January temperature series. The likely explanation of the experienced, large seasonal difference in the quality of temperature series is that most of the technical and environmental problems are related to the incompleteness of sheltering from direct radiation effects, or to local radiation effects influencing the radiation- and heat-balance in the observing site. These effects are obviously larger in summer than in winter.

At least one significant inhomogeneity was detected in almost each of the series of annual mean temperatures. However, most of the detected shift magnitudes are small, they are around or below 0.5 °C. This result is a consequence of the very low noise level owing to the high spatial coherence and low standard deviation of annual mean temperatures. One may conclude, that the detection of such low inhomogeneities is unnecessary (either the detection is precise or not). However, the right evaluation of the results needs some further considerations: (a) Only few inhomogeneities can be detected with much higher magnitudes than the majority. (b) The identification of medium-size or large inhomogeneities may be affected by lower inhomogeneities in the same series. (c) In the investigation of climate change and climatic variability inhomogeneities of not larger than a few tenth of °C might also affect the conclusions.

The skewness of shift magnitude distribution was found to be positive in each examination. The presence of small inhomogeneities tends to be a very common feature of time series from meteorological observations, and time series with at least one, medium-size or large inhomogeneity likely contain other (usually smaller) inhomogeneities.

It would be useful to know, to what extent the results of the used data base are representative for other data bases (of other countries, other variables). We mention that the way of the creation of reference series may influence the inhomogeneity characteristics presented. To assess the representation of the results shown in this study, further investigations are needed on a larger data base with higher diversity of data types and methodology. However, our long-term aim is to find the best OHOM for homogenizing Hungarian temperature series, and the results shown here provide a proper basis for the testing of homogenization methods with time series whose properties are close to those of observed temperature series in Hungary.

One purpose of this study is to make some steps towards a scientifically correct estimation of the effectiveness of individual OHOMs. In an efficiency testing procedure, simulated data sets with known inhomogeneities must be used for evaluating the differences between the detected and factual inhomogeneities. However, statistical properties of the factual inhomogeneities of simulated series should be similar to those of observed data sets, otherwise the calculated efficiencies might provide false information for practical applications. Therefore, the gained knowledge about the basic statistical properties of detectable inhomogeneities in observed data sets is essential for the assessment of efficiencies. The high frequency of small inhomogeneity occurrences, that is a general experience of this study, must be kept in mind in the development of efficiency testing methods.

The main findings of the study are as follows:

- More than half of the investigated series are inhomogeneous (contains at least 1 significant inhomogeneity). The rate of inhomogeneous series is the highest for annual mean temperatures, and the lowest for January mean temperatures.
- The rate of inhomogeneous series is lower for precipitation totals than for temperature means. However, it does not prove a higher quality for precipitation data, as the relatively low spatial correlation coefficients do not allow to detect inhomogeneities of small magnitudes in precipitation series.
- The statistical characteristics of detected inhomogeneities depend on the OHOM applied, but this dependence is usually lower than that on data quality and spatial correlations.

- The series of January mean temperatures have the best quality, and July temperatures have the worst quality. The likely explanation is that most of the inhomogeneity effects on temperature series are related to changes in microscale radiation processes in the surroundings of the thermometer.
- The serial correlation of relative time series is usually a good indicator of the homogeneity quality of the parent time series. In the class of higher than 0.4 serial correlation, the mean number of the detected change points is 2–3 per time series.
- Contamination with small inhomogeneities seems to be a general attribute of meteorological time series. Thus, beyond a general white noise process, small inhomogeneities may also affect the identification of medium-size and large inhomogeneities. An evaluation of the effectiveness of OHOMs, planned for the future, must take this feature of meteorological time series into consideration.

Acknowledgements—This research was partly funded by the VAHAVA project of the Ministry of Environment and Water, in cooperation with the Hungarian Academy of Sciences, and by the Sky Magic Foundation (Debrecen, Hungary). The author thanks *Tamás Szentimrey* (Hungarian Meteorological Service) for the opportunity to use the original software of MASH in the examinations of the study.

References

Aesawy, A.M. and *Hasanean, H.M.*, 1998: Annual and seasonal climatic analysis of surface air temperature variations at six southern Mediterranean stations. *Theor. Appl. Climatol. 61*, 55-68.

Alexandersson, H., 1986: A homogeneity test applied to precipitation data. *J. Climatol. 6*, 661-675.

Alexandersson, H. and *Moberg, A.*, 1997: Homogenization of Swedish temperature data. Part I: Homogeneity test for linear trends. *Int. J. Climatol. 17*, 25-34.

Alexandrov, V., Schneider, M., Koleva, E., and *Moisselin, J.-M.*, 2004: Climate variability and change in Bulgaria during the 20th century. *Theor. Appl. Climatol. 79*, 133-149.

Buishand, T.A., 1982: Some methods for testing the homogeneity of rainfall records. *J. Hydrol. 58*, 11-27.

Domonkos, P., 2005: Homogenisation of time series of observed environmental variables. In *12th Symposium on Analytical and Environmental Problems*. SZAB, Szeged, Hungary, 109-113.

Domonkos, P. and *Tar, K.*, 2003: Long-term changes in observed temperature and precipitation series 1901-1998 from Hungary and their relations to larger scale changes. *Theor. Appl. Climatol. 75*, 131-147.

Ducré-Robitaille, J-F., Vincent, L.A., and *Boulet, G.*, 2003: Comparison of techniques for detection of discontinuities in temperature series. *Int. J. Climatol. 23*, 1087-1101.

Easterling, D.R. and *Peterson, T.C.*, 1995: A new method for detecting undocumented discontinuities in climatological time series. *Int. J. Climatol. 15*, 369-377.

Jones, P.D. and *Lister, D.*, 2004: The development of monthly temperature series for Scotland and Northern Ireland. *Int. J. Climatol. 24*, 569-590.

Karl, T.R. and *Williams Jr., C.N.*, 1987: An approach to adjusting climatological time series for discontinuous inhomogeneities. *J. Clim. Appl. Meteorol. 26*, 1744-1763.

Kohler, M.A., 1949: On the use of double mass analysis for testing the consistency of meteorological records and for making required adjustments. *B. Am. Meteorol. Soc. 5*, 188-189.

Kyselý, J., 2002: Temporal fluctuations in heat waves at Prague-Klementinum, the Czech Republic, from 1901-1997, and their relationships to atmospheric circulation. *Int. J. Climatol. 22*, 33-50.

Moberg, A. and *Alexandersson, H.*, 1997: Homogenization of Swedish temperature data. Part II: Homogenized gridded air temperature compared with a subset of global gridded air temperature since 1861. *Int. J. Climatol. 17*, 35-54.

Peterson, T.C., Easterling, D.R., Karl, T.R., Groisman, P., Nicholls, N., Plummer, N., Torok, S., Auer, I., Boehm, R., Gullett, D., Vincent, L., Heino, R., Tuomenvirta, H., Mestre, O., Szentimrey, T., Salinger, J., Forland, E.J., Hanssen-Bauer, I., Alexandersson, H., Jones, P. and *Parker, D.*, 1998: Homogeneity adjustments of in situ atmospheric climate data: a review. *Int. J. Climatol. 18*, 1493-1517.

Pettitt, A.N., 1979: A non-parametric approach to the change point problem. *Appl. Statistics 28*, 126-135.

Sneyers, R., 1997: Climate chaotic instability. Statistical determination - theoretical backgrounds. *Environmetrics 8*, 517-532.

Sneyers, R., 1999: Homogenizing time series of climatological observations. *Second Seminar for Homogenization of Surface Climatological Data*. Hungarian Meteorological Service, Budapest, 5-14.

Szentimrey, T., 1999: Multiple Analysis of Series for Homogenization (MASH). *Second Seminar for Homogenization of Surface Climatological Data*. Hungarian Met. Service, Budapest, 27-46.

Tomozeiu, R., Busuioc, A., and *Stefan, S.*, 2002: Changes in seasonal mean maximum air temperature in Romania and their connection with large-scale circulation. *Int. J. Climatol. 22*, 1181-1196.

Türkes, M., Sümer, U.M., and *Demir, I.*, 2002: Re-evaluation of trends and changes in mean, maximum and minimum temperatures of Turkey for the period 1929-1999. *Int. J. Climatol. 22*, 947-977.

Vincent, L.A., 1998: A technique for the identification of inhomogeneities in Canadian temperature series. *J. Climate 11*, 1094-1104.

Wijngaard, J.B., Klein Tank, A.M.G., and *Können, G.P.*, 2003: Homogeneity of 20th century European daily temperature and precipitation series. *Int. J. Climatol. 23*, 679-692.

BOOK REVIEW

Kalnay, E., 2003: **Atmospheric Modeling, Data Assimilation and Predictability**. Cambridge University Press, Cambridge, 341 pages, 73 figures, 4 colored plates.

Dynamic meteorology seems to be a very popular subject for university textbook writers. More than 10 high quality textbooks on the dynamics of the atmosphere have been published in the recent 25 years. It is not the case, however, in the field of numerical weather prediction, one of the most important applications of dynamic meteorology. This long felt need has been recently met by the book of an emblematic person of numerical modeling activities, Eugenia Kalnay, Distinguished University Professor of Meteorology at the University of Maryland, former director of the Environmental Modeling Center (EMC) at NCEP, principal investigator of many succesful projects in the field of predictability, ensemble forecasting, and data assimilation, author of several novel publications. The international science community has been waiting for decades for a comprehensive textbook on atmospheric modeling, and finally Dr. Kalnay has just given us the summary of basic knowledge on this rapidly developing territory of meteorology.

The author discusses all aspects of atmospheric and oceanic computer modeling, including a historical overwiev of the subject, equations of motion and their approximations, a clear description of up-to-date numerical methods, and the determination of initial conditions using weather observations, an important new branch of science known as data assimilation. The book also provides a clear discussion of the problem of predictability and chaos in dynamical systems, and investigates how this knowledge can be applied to atmospheric and oceanic modeling. The text touches on the discussion of ensemble forecasting, ENSO events, and the possibility of the improvement of weather and climate prediction.

All in all, this is the book students, lecturers, and researchers of atmospheric modeling have been waiting for decades.

Gy. Gyuró

GUIDE FOR AUTHORS OF *IDŐJÁRÁS*

The purpose of the journal is to publish papers in any field of meteorology and atmosphere related scientific areas. These may be

- research papers on new results of scientific investigations,
- critical review articles summarizing the current state of art of a certain topic,
- short contributions dealing with a particular question.

Some issues contain "News" and "Book review", therefore, such contributions are also welcome. The papers must be in American English and should be checked by a native speaker if necessary.

Authors are requested to send their manuscripts to

Editor-in Chief of IDŐJÁRÁS

P.O. Box 39, H-1675 Budapest, Hungary

in three identical printed copies including all illustrations. Papers will then be reviewed normally by two independent referees, who remain unidentified for the author(s). The Editor-in-Chief will inform the author(s) whether or not the paper is acceptable for publication, and what modifications, if any, are necessary.

Please, follow the order given below when typing manuscripts.

Title part: should consist of the title, the name(s) of the author(s), their affiliation(s) including full postal and E-mail address(es). In case of more than one author, the corresponding author must be identified.

Abstract: should contain the purpose, the applied data and methods as well as the basic conclusion(s) of the paper.

Key-words: must be included (from 5 to 10) to help to classify the topic.

Text: has to be typed in double spacing with wide margins on one side of an A4 size white paper. Use of S.I. units are expected, and the use of negative exponent is preferred to fractional sign. Mathematical formulae are expected to be as simple as possible and numbered in parentheses at the right margin.

All publications cited in the text should be presented in a *list of references*, arranged in alphabetical order. For an article: name(s) of author(s) in Italics, year, title of article, name of journal, volume, number (the latter two in Italics) and pages. E.g., *Nathan, K.K.,* 1986: A note on the relationship between photo-synthetically active radiation and cloud amount. *Időjárás 90,* 10-13. For a book: name(s) of author(s), year, title of the book (all in Italics except the year), publisher and place of publication. E.g., *Junge, C. E.,* 1963: *Air Chemistry and Radioactivity*. Academic Press, New York and London. Reference in the text should contain the name(s) of the author(s) in Italics and year of publication. E.g., in the case of one author: *Miller* (1989); in the case of two authors: *Gamov* and *Cleveland* (1973); and if there are more than two authors: *Smith et al.* (1990). If the name of the author cannot be fitted into the text: *(Miller,* 1989); etc. When referring papers published in the same year by the same author, letters a, b, c, etc. should follow the year of publication.

Tables should be marked by Arabic numbers and printed in separate sheets with their numbers and legends given below them. Avoid too lengthy or complicated tables, or tables duplicating results given in other form in the manuscript (e.g., graphs)

Figures should also be marked with Arabic numbers and printed in black and white in camera-ready form in separate sheets with their numbers and captions given below them. Good quality laser printings are preferred.

The text should be submitted both in manuscript and in electronic form, the latter on diskette or in E-mail. Use standard 3.5" MS-DOS formatted diskette or CD for this purpose. MS Word format is preferred.

Reprints: authors receive 30 reprints free of charge. Additional reprints may be ordered at the authors' expense when sending back the proofs to the Editorial Office.

More information for authors is available: antal.e@met.hu

Information on the last issues: http://omsz.met.hu/irodalom/firat_ido/ido_hu.html

Published by the Hungarian Meteorological Service

Budapest, Hungary

INDEX: 26 361

HU ISSN 0324-6329